Bachelor's Thesis

Bachelor's degree in Industrial Technology Engineering

Modelling and Simulation of an Insular Grid with the presence of High Voltage Direct Current

Author: Ignacio Glenny Crende
Supervisors: Oriol Gomis Bellmunt
Carlos Collados Rodríguez

June 2018

Escola Tècnica Superior
d'Enginyeria Industrial de Barcelona

Abstract

English

Insular electrical grids, usually isolated from larger mainland grids, are more prone to having stability issues. These are usually weak and have limited resources in regards to power sources, which adds up with the fact that this type of grids usually lack access to the electricity market. High Voltage Direct Current (HVDC) technology presents the possibility of long distance overseas connections that alleviate the effects of these issues.

Use of HVDC technology is on the rise, its main focus being long distance transport of power. Its efficiency and the stability it provides to grids, paired with the aforementioned need for overseas connections and off-shore wind generation have helped it become as common as it is nowadays.

The aim of this thesis is to study the behaviour of an insular grid with the presence of HVDC and the needed power converter for the HVDC connection. The behaviour of the system with and without the converter's frequency support will be analyzed.

A case based on the Majorcan 220kV grid (Balearic Islands, Spain) with an HVDC connection representing a link with the mainland is used to analyze the behaviour of an insular grid with and without the frequency support.

HVDC presence in the grid is represented by a converter modelled as seen in *"Active and Reactive Power Control of Grid Connected Distributed Generation Systems"* [1].

The tools used for modelling and simulating are MatLab® 2015b and PSCAD 4.6 EDU.

MatLab® is used for running steady state simulations of the grid's behaviour and for initial modelling of the VSC converter. For the first, the MATPOWER X.Y package is used. In regards to the former, the Simulink environment is used.

PSCAD is used for dynamic analysis of the grid, with and without the power converter's grid frequency support.

Comparison of the MatLab® 2015b and PSCAD 4.6 EDU simulations show that the dynamic model behaves as it is expected from it. There are no relevant differences from the dynamic and the static models' results.

The study of the dynamic behaviour of the system in front of a fault shows that the HVDC connection's grid frequency support alleviates the negative impact that said events have on the grid's frequency. This is done while also reducing the amount of power that needs to be generated with the limited local resources.

Castellano

Las redes eléctricas insulares, generalmente aisladas de las redes continentales, son más dadas a tener problemas de estabilidad. Éstas suelen ser débiles y cuentan con recursos limitados en lo que se refiere a fuentes de energía, lo que se suma al hecho de que éstas redes suelen carecer de acceso al mercado energético. La tecnología de corriente continua de alto voltaje (HVDC por sus siglas en inglés) introduce la posibilidad de conexiones de larga distancia a través de masas de agua que atenuan los efectos de éstos inconvenientes.

El uso de es cada día más común, siendo su principal función el transporte de energía a través de largas distancias. Su eficiencia, junto con la estabilidad que ofrece a las redes y la ya mencionada necesidad de conexiones capaces de atravesar grandes masas de agua han permitido que su uso sea tan extendido en la actualidad.

El objetivo de esta tesis es estudiar el comportamiento de una red insular con presencia de Corriente Continua de Alto Voltage . Se tiene en cuenta al modelar y simular la presencia y el comportamiento del convertidor de control de fuente de voltaje que permite la conexión entre corriente alterna y corriente continua.

Un caso basado en la red eléctrica mallorquina de 220kV (Mallorca, Islas Baleares, España) con una conexión HVDC representando el enlace con el continente es usado para analizar el comportamiento de la red con y sin apoyo de frecuencia.

La presencia de HVDC en la red se muestra mediante un convertidor VSC modelado tal y como se ve en *"Active and Reactive Power Control of Grid Connected Distributed Generation Systems"* [1].

Las herramientas usadas para simular son MatLab® 2015b y PSCAD 4.6 EDU.

MatLab® se usa para las simulaciones de estado estacionario de flujos de potencia. También se usa para un análisis inicial del comportamiento del PLL y el CLC del convertidor VSC. Para el primero se usa MATPOWER, mientras que para los bucles del convertidor se usa SimuLink.

PSCAD se usa para el análisis dinámico de la red, con y sin el convertidor y la correspondiente conexión HVDC.

Si se comparan las simulaciones hechas en MatLab® 2015b y PSCAD 4.6 EDU se puede apreciar que el modelo dinámico se comporta como se espera de él. No hay diferencias relevantes en lo que se refiere a los resultados de los análisis de los modelos dinámico y estático.

El estudio del comportamiento dinámico del sistema ante una falla muestra que el apoyo de frecuencia que provee la conexión HVDC reduce el impacto negativo que tienen tales eventos en la frecuencia de la red. Esto se consigue a la vez que se reduce la cantidad de potencia que ha de ser generada con los recursos limitados de un sistema insular.

Contents

Glossary

AC Alternate Current. xi, 2, 3, 4, 16, 23, 30, 56

CCGT Combined Cycle Gas Turbine. 9, 16, 17, 30, 55

CLC Current Loop Control. ii, xi, 21, 24, 25

DC Direct Current. 2, 3, 4

HVDC High Voltage Direct Current. i, ii, 2, 3, 4, 16, 17, 21, 30, 39, 40, 41, 51, 56

IEEE® Institute of Electrical and Electronics Engineers. 35

p.u. Per Unit. ix, 7, 8, 18, 35, 39, 40

PI Proportional Integral control. 26, 28

PLL Phase Locked Loop. ii, xi, 21, 25, 26, 28, 43

PV Photo-voltaic. 1, 9, 16, 18, 30, 41, 56

VSC Voltage Source Converter. i, xi, 21, 23, 28, 43, 45, 46

List of Tables

List of Figures

Chapter 1

Introduction

1.1 Insular grids

1.1.1 Definition of an insular grid

An islanded or isolated grid corresponds to an electrical power system located in geographical locations that are physically isolated; the most common examples are islands, like Cyprus or Majorca. An insular grid is the particular case of an isolated grid located in an island.

Generally, insular grids are comprised by few traditional fuel-based generation installations. The Spanish islands Majorca and Tenerife are good examples of this situation. Majorca, home to nearly 870000 people in the Mediterranean, has four main generating installations with a total rated power of 1527 MW [2]. Tenerife, where nearly 890000 people live to the west of the moroccan coast, counts with an installed rated power of 944 MW distributed among five different generators (in addition to nearly 60MW of Photo-voltaic generation [3].

As a result, insular power systems present a significantly low inertia when compared to the continental grid. This makes them unreliable especially when taking into account possible outages or fuel shortages.

1.1.2 The fuel dependency issue

The dependence on fuel imports is also a noticeable issue with insular grids. Isolated and with limited resources, an island's electricity production is usually heavily dependent on foreign gasoline, oil or liquefied petrol gas.

Such resources are generally transported by tankers; as a result transportation costs make electricity production more expensive. This transport also means that the environmental effects of fossil fuel based generation are aggravated [4].

To add up, losses tend to be higher in insular areas due to the aged, low quality systems, thus promoting increases of fuel utilization and the unit cost of electricity [4].

1.1.3 Reliability of insular grids

Another problematic present in insular grids is their fragility in comparison to mainland grids. A specially relevant factor is their lower inertia; this is because there are less generating facilities connected to the system and an insufficient (sometimes completely lacking) interconnection with the main grid [4].

Generally, insular grids present a certain lack of meshing, sometimes going as far as being single-line based. This translates into faults being even more serious, since losing certain connections may cut all power supply to certain areas.

As a result, insular grids are more sensitive to frequency and voltage deviations, thus affecting power quality. This vulnerability reduces system reliability and security.

A clear indicator of a grids unreliability can be the energy that has not been supplied, and the Spanish situation exemplifies this perfectly; in 2017 more than an 87% of the energy not supplied in Spain concerned the Canary Islands [5].

1.1.4 Renewable energy sources integration

A natural response to fuel dependency is the implementation of renewable energy sources such as solar or wind power [6]. This would also imply a reduction in CO_2 emissions.

But these energy sources present an intermittence and unreliability that in turn affects the grid frequency negatively; this is of particular importance in small, fragile systems like insular grids.

As a result, network security and their interruptible nature are limiting the implementation of renewable energy sources in insular grids [4]. This is currently slowing down their introduction as a reliable solution to the fuel imports dependency issue.

1.2 The role of HVDC

Until AC/DC power converters arrived, it was not commercially viable to use long-distance DC lines to transport energy. Now, with AC already settled, High Voltage Direct Current (HVDC) connections present themselves as an important alternative for bulk transport of electricity through long distances, especially overseas.

1.2.1 Advantages of HVDC connections

The main advantages of HVDC transmission, exemplified with installations that will be further explained in section 1.2.3, are as follows:

1. *HVDC allows for more reliable and cheaper asynchronous connections.* The Garabi 2000 MW Interconnection HVDC transmission allows the connection of grids working at completely different frequencies, as is the case with the Argentinean (50 Hz) and Brazilian (60 Hz) grids [7–9].

2. *HVDC improves grid security and stability.* The Quebec-New England HVDC transmission was unaffected by the 2003 power outage that propagated through the Lower Lakes, Ontario and New York (United States). This meant that even if the New York-New England AC interconnection tripped, the HVDC transmission from Quebec was still able to deliver power to New England [8, 9].

3. *HVDC allows for longer underwater connections.* With extremely high shunt capacitance insulated cables, the limit for AC connections underwater is around 100 km; beyond that distance, HVDC is the only technically viable option [8, 10].

This advantages are in addition to the fact that when traversing long distances High Voltage Direct Current transmission suffers less losses than High Voltage Alternate Current transmission. This is because AC generates reactive power, increasing with distance. Since losses on DC transmission are caused mostly by the converters than the cable itself, for long distances HVDC is preferable [9, 11].

1.2.2 DC technology through the years

Early years

The first commercial central power station appeared in 1879, offering arc-light service to subscribers. Edison's first short range DC systems appear in 1882, with Ganz & Co. and Westinghouse Electric Co. competing offering AC transmissions in Europe and the United States respectively [12, 13].

Edison's DC systems, with its first practical demonstration of incandescent electric lights in 1879 [13], were overshadowed by the capabilities of AC. With a 40 km connection from Turin to the remote Lanzo, the Gaulard-Gibbs AC Distribution System showed how AC was capable of providing electricity to sparsely populated areas, something not possible profitably with Edison's short range DC transmission technique [12].

Appearance and dominance of polyphase systems

Commercial viability of AC arrived with the ZDB (introduced by Ganz & Co. in 1885 and named ZDB because of Kàroly Zipernowsky, Miksa Déri and Ottó Titusz Bláthy.). Westinghouse Electric Co., born in 1886, is the one that brings AC to the United States. AC systems quickly grew in the market; in 1887 there were 20 Westinghouse installations in the United States versus the 103 DC systems of Edison and three years later, in 1890, there were 323 Westinghouse AC systems and 202 DC [12].

Even though AC transmission suffers more losses than DC transmission [11], the lack of converters to be able to tone down the voltage of the latter made High Voltage Direct Current transmissions impractical. Being AC the only practical option for long-distance transmission, polyphase systems shine once longer distances need to be covered and efficiency comes into play; three-phase transmission losses are about 20% less than those of monophase AC transmission [12].

Oskar von Miller showed the capabilities of the three-phase transmission system in 1891. Based on a modification of Tesla's two-phase system, it became a commercial success and was quickly implemented around the world. In 1923 transmission voltages reached 220kV, preceded by several scientific breakthroughs and a steady and continuous rise of said voltages [12].

DC central stations were still used in densely populated areas; the turning point was the implementation of regional power grids. Entering 1922, most DC central stations were converting to AC [12].

Appearance of HVDC

AC generation and distribution are still the norm nowadays, but AC long-distance transmission is challenged by High Voltage Direct Current (HVDC) transmission. This was possible thanks to the introduction of high voltage $AC - DC$ converters. The General Electric Co. developed the first HVDC system in 1936 [12].

1.2.3 High Voltage Direct Current transmission nowadays

The first commercial transmission began in 1954; a 98 km cable at ±100 kV in Sweden with a 20 MW capacity [12]. Nowadays there are several HVDC connections around the world. These are some important examples that show how the advantages explained in section 1.2.1 are taken advantage of nowadays.

1. *The Garabi 2000 MW Interconnection:* between Garabi (Brazil) and Yacyretá (Argentina), a 500 kV transmission line of nearly 500 km in length connects the 500 kv networks. Using back-to-back HVDC frequency converters installed in Garabi, the connection links two weak points of the Argentinean 50 Hz grid and the Brazilian 60 Hz [7]. Beginning commercial operation in 1999 and 2002, the project is divided in two 1100 MW separate phases [14].
2. *The Quebec–New England Transmission:* it is one of the two remaining multi-terminal HVDC systems in the world. The transmission first went into service back in 1986, with a 690 MW capacity and a ±450 kV operating voltage. Nowadays it counts with five different connections, the most notable among them being the Radisson-Nicolet one with a 2000 MW capacity [15, 16].
3. *Project Rómulo:* connecting Sagunto (Valencia, Spain) and Majorca (Balearic Islands, Spain) and supplying power while improving reliability, quality and stability of the latter [17], it is an underwater 237 km connection submerged at a maximum depth of 1485 m with a 400 MW capacity ($2x200$ MW) that started operating in 2012 [17].

1.3 Objectives and scope

The main objective of the thesis is to study the behaviour of an insular grid with High Voltage Direct Current (HVDC) presence.

The simulation and analysis process has been divided into four different parts:

1. *A steady-state simulation of the grid*, studying its power flow and analyzing voltage and phase, done with MatLab® 2015b (MATPOWER [18]).
2. *A dynamic simulation of the grid without droop control on the converter*, studying settling time for the same case simulated in MatLab® and its reaction to a fault, done with PSCAD 4.6.
3. *A dynamic simulation of the grid with droop control on the converter*, studying settling time for the same case simulated in MatLab® and its reaction to a fault, done with PSCAD 4.6.
4. *A comparison of the system's steady state behaviour*, using the MatLab® steady-state simulation and the PSCAD dynamic simulation once steady-state has been reached.
5. *A comparison of the system's behaviour when the fault occurs*, using both dynamic simulations.

Chapter 2

Steady State Analysis: Modelling

In this chapter the models used for the steady-state analysis via MatLab®and the methodology the resolution is based on are explained. The purpose of the steady state simulation is to do a power flow analysis of the grid.

2.1 Per Unit (p.u.) system

The Per Unit (p.u.) system is used for simplifying calculations and readings related to electrical power systems. The main advantages of the p.u. system are as follows:

- *Values of the same variable (voltage, current...) are similar.* This simplifies the comparison of systems that differ in size.
- *Calculations are simpler.* Some systems require you to take into account different voltage levels (i.e. working with a transformer). By using different p.u. base values, bringing the different voltage values to a similar scale, the calculations are simplified significantly.
- *Three-phase calculations are simplified.* Some expressions used in most three-phase calculations disappear when working in p.u., simplifying both calculations and expressions.

The corresponding values in p.u. are obtained by dividing the actual value in the standard *abc* reference by a predefined base value. The different base values S_B, V_B, I_B and Z_B (for apparent power, tension, current and impedance) are related via the following equations:

$$S_B = \sqrt{3} V_B I_B \tag{2.1}$$

$$V_B = \sqrt{3} Z_B I_B \tag{2.2}$$

$$I_B = \frac{S_B}{\sqrt{3} V_B} \tag{2.3}$$

$$Z_B = \frac{V_B}{\sqrt{3} I_B} = \frac{V_B^2}{S_B} \tag{2.4}$$

Once the base values are defined, calculating the p.u. equivalent s, v, i and z of the standard values S, V, I and Z is done by calculating the quotient of the standard value divided by the base value.

$$s = \frac{S}{S_B} \tag{2.5}$$

$$v = \frac{V}{V_B} \tag{2.6}$$

$$i = \frac{I}{I_B} \tag{2.7}$$

$$z = \frac{Z}{Z_B} \tag{2.8}$$

MATPOWER [18], the MatLab® program used for the steady state analysis of the grid, uses p.u. for its calculations. Base power S_B and base voltage V_B values are input by the user. As seen in equations 2.1-2.4, all base values are already defined when two are.

2.2 Transmission lines

Lines are implemented following an RL model. A characteristic impedance per unit of length z_0 $[\Omega/km]$ is defined as seen in equation 2.9, where f is the grid frequency $[rad/sec]$.

By multiplying this value per each defined length as in equation 2.10, different line impedances are calculated. These lengths are defined as l_{Xx-y} $[km]$, where X and x refer to the buses the line connects and y, optional, denotes different lines that connect a same pair of buses.

$$z_0 = 0.144 + j \cdot 1.35 \cdot 10^{-3} \cdot f \tag{2.9}$$

$$Z_{Xx-y} = l_{Xx-y} \cdot z_0 \tag{2.10}$$

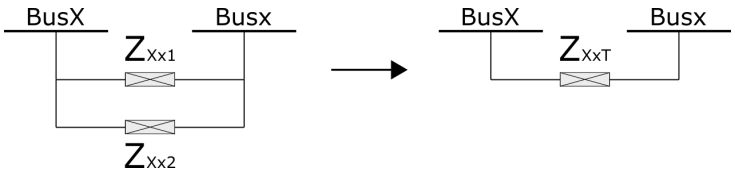

Figure 2.1: Visual representation of two buses connected by two separate transmission lines and its equivalent.

Aiming to simplify the model by reducing the number of transmission lines, when two parallel transmission lines are operating between the same nodes as seen in figure 2.1 the equivalent impedance Z_{XxT} is calculated as seen in equation 2.11.

$$Z_{XxT} = \frac{Z_{Xx-1} \cdot Z_{Xx-2}}{Z_{Xx-1} + Z_{Xx-2}} \tag{2.11}$$

2.3 Loads

Loads for the steady state simulation are modelled as a specified constant quantity of complex power consumed at a bus [19]. The loads considered in this thesis are all of a purely resistive nature.

2.4 Generation

Generation for the initial steady state simulation is modelled as a complex power injection at a specific bus [19].

The simplicity of this model allows for the implementation of Photo-voltaic (PV) generation, which has been disregarded during the dynamic analysis.

Combined Cycle Gas Turbine (CCGT) and classical thermal power generation, implemented in both steady state and dynamic studies, represent the main power sources of the grid.

2.5 Resolution process

2.5.1 Type of buses

Depending on their function and what values are fix, three different types of buses are used [19]:

- *Slack buses* serve the role of voltage phase reference and real power slack. Only one slack bus must be defined.
- *PV buses* are the remaining buses with classical generation. In these, the voltage magnitude and the real power injection applied by the generator are fixed.
- *PQ buses* are all non-generating buses. In these, both real and reactive power consumption are fix and specified.

2.5.2 Resolution method

The basis of the resolution method is set with equation 2.12.

$$[Y][V] = [J] \tag{2.12}$$

Where matrix $[Y]$ is the admittance matrix $[1/\Omega]$, $[V]$ is the voltages matrix $[V]$ and $[J]$ is the currents matrix $[A]$.

Each diagonal k-th term of the admittance matrix $[Y]$ is defined as the sum of all admittances connected to k bus.

Each term in a given (j, k) position is defined as the sum of all admittances, changing their sign, between both buses k and j.

Given a general situation with n buses, the $[Y]$ matrix would be defined as follows:

$$[Y] = \begin{bmatrix} Y_1 & -Y_{12} & ... & -Y_{1k} & ... & -Y_{1(n-1)} & -Y_{1n} \\ -Y_{21} & Y_2 & ... & -Y_{2k} & ... & -Y_{2(n-1)} & -Y_{2n} \\ ... & ... & & ... & & ... & ... \\ -Y_{k1} & -Y_{k2} & ... & Y_k & ... & -Y_{k(n-1)} & -Y_{kn} \\ ... & ... & & ... & & ... & ... \\ -Y_{(n-1)1} & -Y_{(n-1)2} & ... & -Y_{(n-1)k} & ... & Y_{(n-1)} & -Y_{(n-1)n} \\ -Y_{n1} & -Y_{n2} & ... & -Y_{nk} & ... & -Y_{n(n-1)} & Y_n \end{bmatrix} \tag{2.13}$$

The $[Y]$ matrix is symmetrical. This translates into the non-diagonal terms being equal as in $-Y_{12} = -Y_{21}$. The final expression of the $[Y]$ matrix would be

$$[Y] = \begin{bmatrix} Y_1 & -Y_{12} & ... & -Y_{1k} & ... & -Y_{1(n-1)} & -Y_{1n} \\ -Y_{12} & Y_2 & ... & -Y_{2k} & ... & -Y_{2(n-1)} & -Y_{2n} \\ ... & ... & & ... & & ... & ... \\ -Y_{1k} & -Y_{2k} & ... & Y_k & ... & -Y_{k(n-1)} & -Y_{kn} \\ ... & ... & & ... & & ... & ... \\ -Y_{1(n-1)} & -Y_{2(n-1)} & ... & -Y_{k(n-1)} & ... & Y_{(n-1)} & -Y_{(n-1)n} \\ -Y_{1n} & -Y_{2n} & ... & -Y_{kn} & ... & -Y_{(n-1)n} & Y_n \end{bmatrix} \tag{2.14}$$

Since transmission lines in this thesis are modelled following an impedance-based RL model, the equivalent admittance Y_{Xx} of each impedance Z_{Xx} must be calculated (see equation 2.15) in order to solve the system.

$$Y_{Xx} = \frac{1}{Z_{Xx}} \tag{2.15}$$

Each term of the potential vector $[V]$ is the voltage assigned to each bus in volts $[V]$. Given a general situation with n buses, the $[V]$ vector would be defined as follows:

$$[V] = \begin{bmatrix} V_1 \\ V_2 \\ ... \\ V_{n-1} \\ V_n \end{bmatrix} \tag{2.16}$$

Each term of the currents vector $[J]$ equals the algebraic sum of the ideal current sources entering a given k bus in $[A]$. Values are considered positive when the current is entering the given bus k and negative when they come out of the bus.

Considering a system with n buses, the $[J]$ vector would be defined as follows:

$$[J] = \begin{bmatrix} J_1 \\ J_2 \\ ... \\ J_{n-1} \\ J_n \end{bmatrix} \tag{2.17}$$

The value of these ideal current sources is determined by the voltage of the bus and the load and generation applied to it.

For a given bus k with a line-to-line voltage V_k $[V]$, an apparent three-phase power generation S_{kgen} and an apparent three-phase power consumption S_{kcon} $[VA]$, the total value of the current J_k $[A]$ that enters or comes out of the bus is calculated as seen in equation 2.18 below.

$$\begin{aligned} J_k &= J_{kgen} + J_{kcon} \\ &= \frac{S_{kgen}/3}{V_k/\sqrt{3}} + \frac{-S_{kcon}/3}{V_k/\sqrt{3}} \\ &= \frac{S_{kgen}}{V_k\sqrt{3}} + \frac{-S_{kcon}}{V_k\sqrt{3}} \end{aligned} \tag{2.18}$$

J_{kgen} and J_{kcon} represent the equivalent ideal current sources for S_{kgen} and S_{kcon} respectively.

2.5.3 Loss calculation

Once the aforementioned system has been resolved, it is possible to calculate the current that goes through each transmission line and the losses due to Joule heating (also known as ohmic heating or resistive heating).

As stated by Joule's first law, the power of heating P_{loss} $[W]$ generated by a conductor is calculated as seen in equation 2.19 below.

$$P_{loss} = I_{Xx}^2 \cdot R_{Xx} \tag{2.19}$$

Where I_{Xx} is the absolute value (or modulus) of the current that goes from bus X to bus x and R_{Xx} is the real part of the complex value of the impedance Z_{Xx} that connects the aforementioned X and x buses.

The current I_{Xx} between buses X and x is calculated once the potential of the buses has been obtained, and follows equation 2.20.

$$I_{Xx} = \frac{V_X - V_x}{Z_X x} \tag{2.20}$$

Chapter 3

Steady State Analysis: Case, simulation and results

3.1 Case

The modelling and simulations are done with a grid model based on the Majorcan grid. Ten different buses are defined based on the ones seen in *Red Eléctrica de España*'s Majorcan grid map [2].

Using *Red Eléctrica de España*'s grid maps [2] and Google Maps' Measure Distance tool, the different components that shape the grid are defined. A schematic representation of the modelled grid studied in this case can be seen in figure 3.1.

3.1.1 Lines

An approximate trace of the transmission lines seen in *Red Eléctrica de España*'s grid maps [2] was done in Google Maps using its Measure Distance tool. These lengths are defined as l_{Xx-y} $[km]$, where X and x refer to the buses the line connects and y, optional, denotes different lines that connect a same pair of buses. By applying equation 2.10, seen in 2.2, the value of the characteristic impedance of each line is obtained. The resulting lengths and impedances can be seen in tables 3.1 and 3.2.

As mentioned in 2.2, some buses are connected with two transmission lines. These can be simplified into one by calculating the equivalent impedance following equation 2.11. The affected lines and their corresponding values can be seen in table 3.3.

3.1.2 Loads

Most loads are initially defined as a function of the population. For this purpose, the total Majorcan population (868692 inhabitants) [20] is divided in 3 main groups:

1. *The Majorcan capital*, where roughly half of the island's population resides (406492 inhabitants) [20, 21].

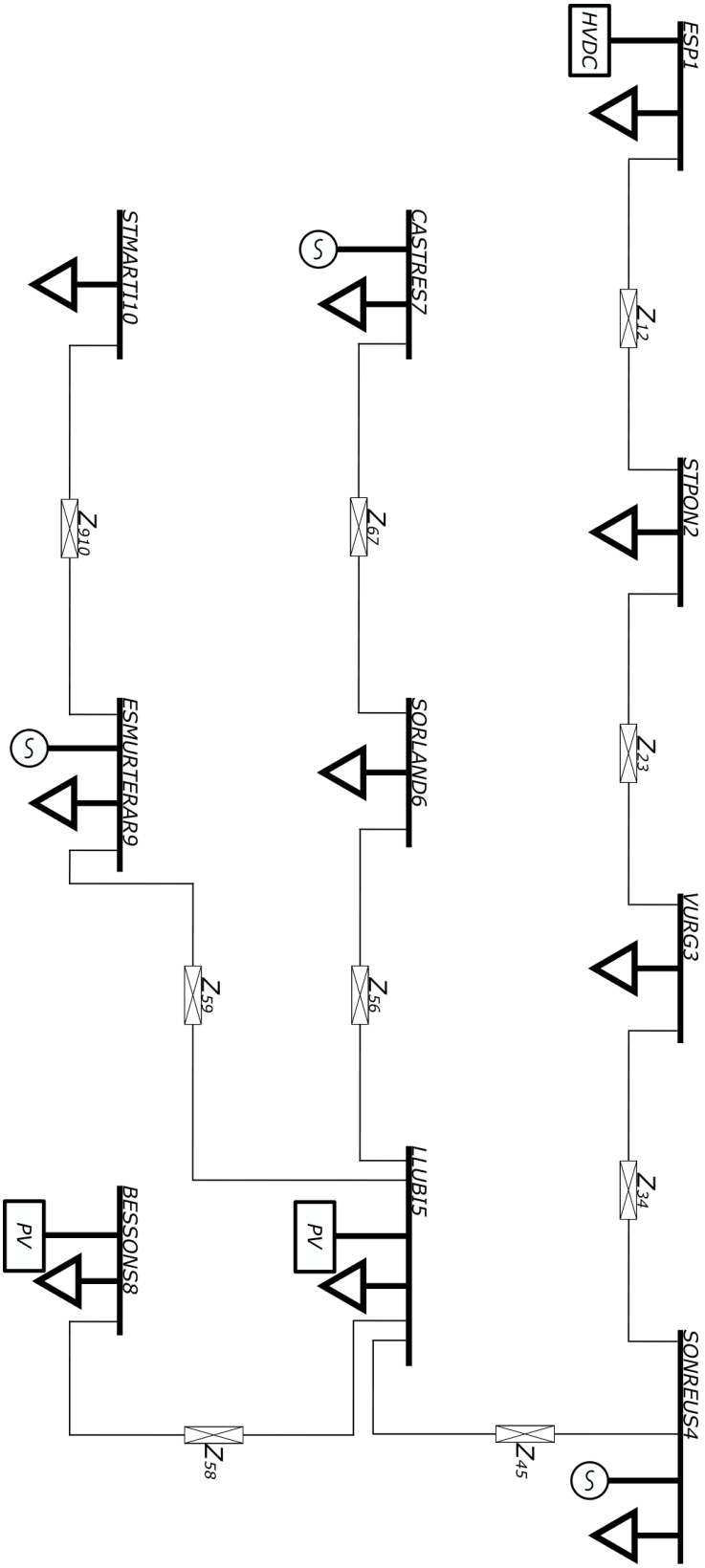

Figure 3.1: Schematic representation of the grid, representing the different buses, loads, power sources, transmission lines and line impedances.

Table 3.1: Length of each transmission line as defined in the model.

Line	Length (km)
l_{12}	1.034
l_{23}	5.17
l_{34-1}	15.16
l_{34-2}	15.16
l_{45}	38.62
l_{46}	6.29
l_{65}	29.8
l_{67-1}	10.14
l_{67-2}	10.14
l_{58-1}	12.81
l_{58-2}	12.13
l_{59-1}	20.11
l_{59-2}	16.84
l_{910-1}	2.8
l_{910-2}	2.8

Table 3.2: Characteristic impedance of each transmission line as defined in the model. [Ω]

Impedance	Characteristic Impedance Value [Ω]
Z_{12}	$0.1489 + j \cdot 0.4385$
Z_{23}	$0.7445 + j \cdot 2.1927$
Z_{34-1}	$2.1830 + j \cdot 6.4296$
Z_{34-2}	$2.1830 + j \cdot 6.4296$
Z_{45}	$5.5613 + j \cdot 16.3793$
Z_{46}	$0.9058 + j \cdot 2.6677$
Z_{65}	$4.2912 + j \cdot 12.6386$
Z_{67-1}	$1.4602 + j \cdot 4.3005$
Z_{67-2}	$1.4602 + j \cdot 4.3005$
Z_{58-1}	$1.8446 + j \cdot 5.4329$
Z_{58-2}	$1.7467 + j \cdot 5.1445$
Z_{59-1}	$2.8958 + j \cdot 8.5290$
Z_{59-2}	$2.4250 + j \cdot 7.1421$
Z_{910-1}	$0.40332 + j \cdot 1.1875$
Z_{910-2}	$0.40332 + j \cdot 1.1875$

Table 3.3: Equivalent characteristic impedance of each affected transmission line. [Ω]

Line Impedance	Equivalent Impedance Value [Ω]
Z_{34T}	$1.0915 + j \cdot 3.2148$
Z_{58T}	$0.7301 + j \cdot 2.1503$
Z_{59T}	$0.8972 + j \cdot 2.6424$
Z_{67T}	$1.3198 + j \cdot 3.8871$
Z_{910T}	$0.2016 + j \cdot 0.5938$

2. *Other highly populated municipalities*, like Inca or Manacor among others. These are used for distributing the population of the rural area of the island in a more heterogeneous way [21].

3. *The rest of the population* has been divided among the total number of buses minus one and then applied to those. This is because the first bus is not considered as populated because it represents the connection with Ibiza and the HVDC connection with Sagunto.

February 5*th*'s peak demand [22] was used in order to define the analyzed working points of the grid, with the load being calculated following equation 3.1.

$$P_{consbus} = \frac{P_{total}}{Pob_{tot}} \cdot Pob_{bus} \tag{3.1}$$

The load of the bus that presents both the HVDC connection with the Iberian Peninsula and the AC connection with Ibiza is calculated differently. In the MatLab® steady state simulation, the values used are as seen on February 5*th*'s peak demand [22].

Table 3.4 shows the population Pob_{bus} and peak load Ld_{pk} $[MW]$ both total and for each bus. The percentage of the total load $\%Ld$ that belongs to each defined bus is also included.

Table 3.4: Name, bus index, population, percentage of the total load of the grid and for each defined bus. The last instance is the island's total.

Name	Bus index	Pob_{bus}	$\%Ld$	$Ld_{pk}[MW]$
Link Santa Ponça	ESP1	0	1.09	7.6
Santa Ponça	STPON2	21129	2.41	17.1
Valldurgent	VURG3	179992	20.49	144.9
Son Reus	SONREUS4	129629	14.76	104.3
Llubí	LLUBI5	36429	4.15	29.3
Sant Orlandís	SORLAND6	215077	24.49	173.1
Cas Tresorer	CASTRES7	129629	14.76	104.4
Es Bessons	BESSONS8	78693	8.96	63.4
Es Murterar	ESMURTERAR9	21129	2.41	17.1
Sant Martí	STMARTI10	56985	6.48	45.8
Majorca	-	868692	100	707

Reactive power consumption has been considered null, meaning that the different loads have a power factor $cos(\varphi) = 1$.

3.1.3 Generation

In order to define the generation of the different buses, demand as seen on February 5*th*'s peak [22] was used. The % of energy produced from each source (Photo-voltaic, Combined Cycle Gas Turbine, classical thermal and fed through the HVDC link) can be obtained from *Red Eléctrica de España*'s real-time demand tracking service [22].

In [2] four different CCGT and classical thermal sources are mentioned; a classical thermal and a CCGT at the bus SONREUS4 of a rated power of $135MW$ and $429MW$ each, a CCGT of a rated power of $429MW$ at CASTRES7 and a $534MW$ classical thermal station at the bus $ESESMURTERAR9$.

Table 3.5 shows the power mix for the peak and how the generation is distributed among the different buses. Also, in table 3.6 the total generation assigned to each bus and the percentage of the total it represents are shown.

Table 3.5: Different energy sources used at each generating bus for peak consumption. The last instance is the island's total.

Bus index	PV $[MW]$	Thermal $[MW]$	CCGT $[MW]$	HVDC Link
ESP1	0	0	0	231.8
SONREUS4	0	81.3	67.5	0
LLUBI5	7.6	0	0	0
CASTRES7	0	0	67.5	0
BESSONS8	7.6	0	0	0
ESESMURTERAR9	0	243.7	0	0
-	15.2	325	135	231.8

Table 3.6: Total generation of each bus when supplying for the peak load and % of total generation in the grid for each bus. The last instance is the island's total.

Bus index	Total [MW]	% of Total Generation
ESP1	231.8	32.78
SONREUS4	148.8	21.04
LLUBI5	7.6	1.06
CASTRES7	67.5	9.55
BESSONS8	7.6	1.06
ESESMURTERAR9	243.7	34.46
-	707	100

3.2 Simulation and results

Using MATPOWER [18] via MatLab, steady state simulations can be done fast, allowing us to quickly analyze the system's response in regards to losses, where does the power flow from and to and which are the parts of the grid subject to higher voltage deviations.

Buses with CCGT and traditional thermal generation are all defined as PV buses (fixed real power injection and voltage magnitude) except for *ESESMURTERAR9* that functions as real power slack and voltage phase reference. Bus *ESP1*, representing the HVDC link, has been defined as a PQ bus.

Since *ESESMURTERAR9* serves the real power slack purpose, its simulated power generation does not match the one calculated for it in subsection 3.1.3. The difference between the simulated generation and the theoretical one is the power lost in transmission due to Joule heating, which

was not considered when defining generation and loads. Buses without generation are all defined as PQ buses (fixed real and reactive power consumption).

Table 3.7: Voltage V of each bus in $p.u.$, the difference between a bus and the slack's phase $\Delta\varphi$ in $degrees$, active power generation P_g $[MW]$, reactive power generation Q_g $[MVAR]$.

Bus index	V $[p.u.]$	$\Delta\varphi$ $[deg]$	P_g $[MW]$	$Q_g[MVAR]$
ESP1	1.005	-0.780	231.80	-3.70
STPON2	1.004	-0.895	-	-
VURG3	1.001	-1.426	-	-
SONREUS4	1.000	-1.658	148.80	-3.32
LLUBI5	0.998	-0.907	7.60	0.00
SORLAND6	0.998	-2.117	-	-
CASTRES7	1.000	-2.252	67.50	46.66
BESSONS8	0.997	-1.082	7.60	0.00
ESMURTERAR9	1.000	+0.000	246.64	-38.15
STMARTI10	1.000	-0.032	-	-

In table 3.7 the results of the steady state simulation are shown. Voltages, represented in p.u., match the nominal value of $220kV$ at the generating buses *SONREUS4*, *CASTRES7* and *ESMURTERAR9*, the latter's phase being null because it functions as voltage reference.

Disregarding the PV generation in buses *LLUBI5* and *BESSONS8*, where reactive power generation/consumption has been forced to zero, all power sources show reactive power exchanges. These cover the reactive power needed because of the inductive behaviour of the RL transmission line model and the reactive power used to control the voltage at buses *SONREUS4*, *CASTRES7* and *ESMURTERAR9*.

Power factors for buses *ESP1*, *SONREUS4*, *CASTRES7* and *ESMURTERAR9* are calculated as $cos(\varphi) = P_g/\sqrt{P_g^2 + Q_g^2}$.

In general, power factors are higher than $cos(\varphi) = 0.98$. The only generating bus that stands out is *CASTRES7* with a power factor $cos(\varphi) = 0.8226(i)$. It is also the only inductive power factor among the different power supply buses.

In figure 3.2, a schematic representation of the system's power flow for the defined case can be appreciated.

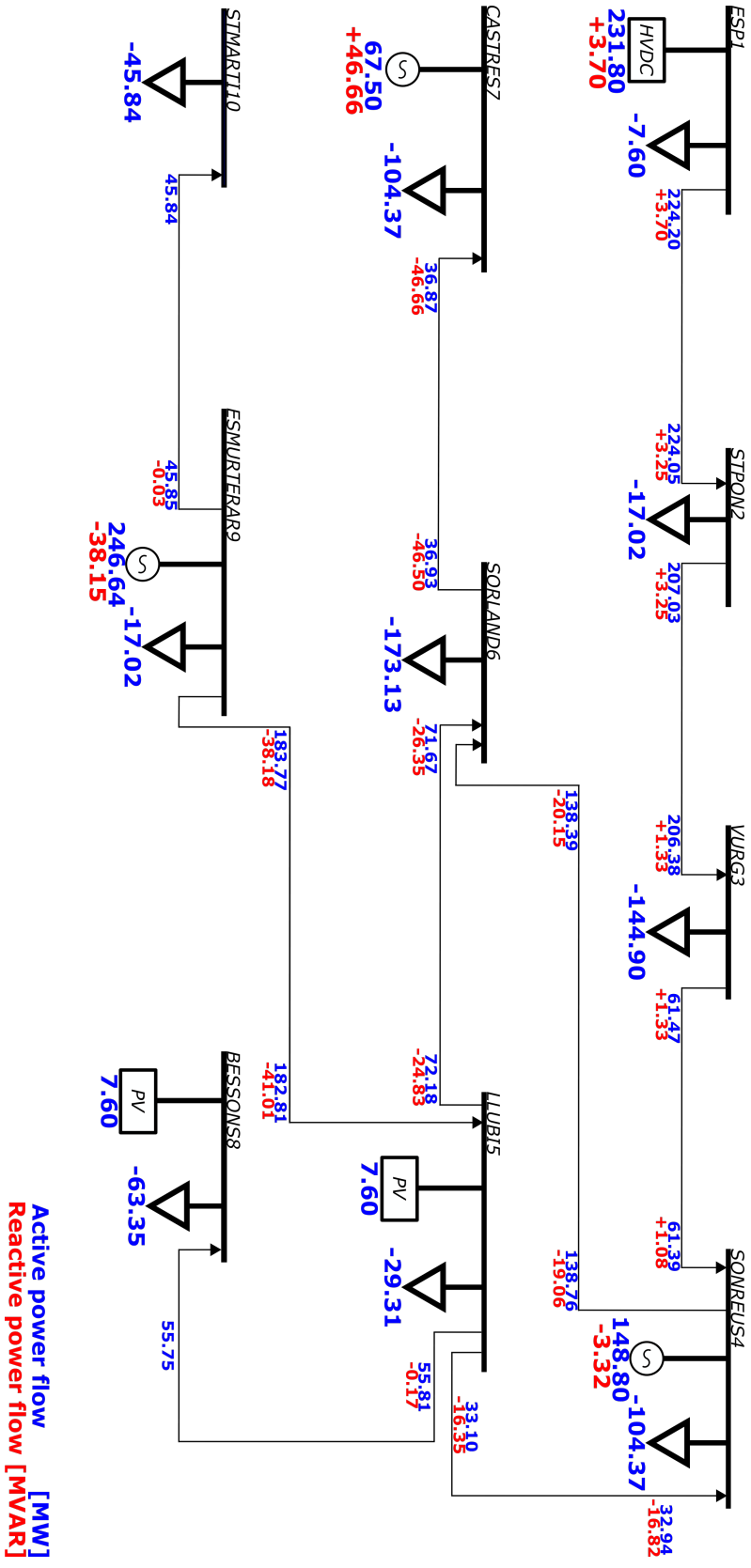

Figure 3.2: Power flow diagram of the peak demand case representing the values obtained via the MatLab® steady-state simulation.

Chapter 4

Dynamic Analysis: Modelling

In this chapter the models that form the different components of the grid are explained. All the implemented control methods are also detailed.

The transmission line model is not explained because it is the same as the one implemented in the steady state simulation seen in 2.2.

4.1 Voltage Source Converter

As explained in 1.2, power converters are needed when working with High Voltage Direct Current transmissions. The Sagunto-Majorca HVDC link is represented in the modelled grid as the power converter station on the island's end. A two-level Voltage Source Converter (VSC) is implemented using an average model implementing the Phase Locked Loop (PLL) and the Current Loop Control (CLC) described in *"Active and Reactive Power Control of Grid Connected Distributed Generation Systems"* [1].

4.1.1 The Park transformation

When working on the *abc* frame, some magnitudes present an oscillating nature that complicates the implementation of control systems like the Phase Locked Loop (PLL) or the Current Loop Control (CLC) used in the VSC.

By using the Park transformation and working on the so-called synchronous reference frame it is possible to read this oscillating values as constant quantities [1, 23].

The Park transformation can be defined as the combination of a geometrical transformation that changes the vectors from the standard *abc* reference frame to an ortogonal $\alpha\beta 0$ reference frame (Clarke transformation) and a rotation (θ). This can be appreciated in Figure 4.1.

When a balanced three-phase voltage system is considered, the v_0 component of both the $\alpha\beta 0$ and the $qd0$ reference frames is null.

The Park transformation is given by equation 4.1 below.

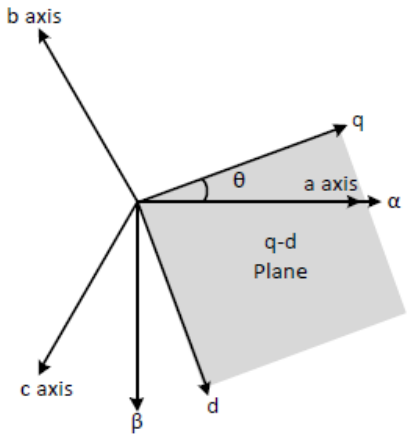

Figure 4.1: qd plane representation [1].

$$[x_{qd0}] = [T_{qd0}][x_{abc}] \tag{4.1}$$

Where x_{qd0} represents the different magnitudes expressed in the $qd0$ reference frame and x_{abc} the same magnitude in the abc frame. The transformation matrix $T_{qd0} = T(\theta)$ and the inverted matrix $T_{qd0}^{-1} = T^{-1}(\theta)$ are defined as follows.

$$T(\theta) = k \begin{bmatrix} cos(\theta) & cos(\theta - \frac{2\pi}{3}) & cos(\theta + \frac{2\pi}{3}) \\ sin(\theta) & sin(\theta - \frac{2\pi}{3}) & sin(\theta + \frac{2\pi}{3}) \\ \frac{1}{2} & \frac{1}{2} & \frac{1}{2} \end{bmatrix} \tag{4.2}$$

$$T^{-1}(\theta) = k \begin{bmatrix} cos(\theta) & sin(\theta) & 1 \\ cos(\theta - \frac{2\pi}{3}) & sin(\theta - \frac{2\pi}{3}) & 1 \\ cos(\theta + \frac{2\pi}{3}) & sin(\theta + \frac{2\pi}{3}) & 1 \end{bmatrix} \tag{4.3}$$

By defining θ as the electrical angle, constant steady state quantities are obtained instead from what once were the oscillating values of voltage and current [1].

Once the studied variables have undergone the needed control procedures, they are reconverted to the abc reference frame by means of equation 4.4.

$$[x_{abc}] = [T_{qd0}]^{-1}[x_{qd0}] \tag{4.4}$$

If $k = 2/3$, for balanced sinusoidal conditions, the steady state value of current i_q equals the peak value of i_a [23]. This is why for the rest of this thesis $k = 2/3$ will be assumed.

This can be checked by looking at the expression of i_q and i_d as a function of the currents in the abc frame, the angle θ and k in equations 4.5 and 4.6 below. This will be demonstrated with i_q, but it can be applied to i_d too [23]. Given that equations for the individual values of i_q and i_d are being defined, it has been deemed convenient to describe i_0 too, even if it remains unaffected by the constant's value.

$$i_q = k[i_a cos(\theta) + i_b cos(\theta - \frac{2\pi}{3}) + i_c cos(\theta + \frac{2\pi}{3})] \tag{4.5}$$

$$i_d = k[i_a sin(\theta) + i_b sin(\theta - \frac{2\pi}{3}) + i_c sin(\theta + \frac{2\pi}{3})] \tag{4.6}$$

$$i_0 = \frac{1}{3}(i_a + i_b + i_c) \tag{4.7}$$

Equations 4.8-4.10 for i_a, i_b and i_c in balanced conditions have to be substituted into equation 4.5. Doing this results in equation 4.11.

$$i_a = I_m cos(\omega_s t) \tag{4.8}$$

$$i_b = I_m cos(\omega_s t - \frac{2\pi}{3}) \tag{4.9}$$

$$i_c = I_m cos(\omega_s t + \frac{2\pi}{3}) \tag{4.10}$$

$$\begin{aligned} i_q &= k[I_m cos(\omega_s t)cos(\theta) + I_m cos(\omega_s t - \frac{2\pi}{3})cos(\theta - \frac{2\pi}{3}) + I_m cos(\omega_s t + \frac{2\pi}{3})cos(\theta + \frac{2\pi}{3})] \\ &= k\frac{3}{2} I_m cos(\omega_s t - \theta) \end{aligned} \tag{4.11}$$

By substituting $k_d = 2/3$ in equation 4.11, equation 4.12 results, where i_q euqals the peak value I_m of i_a, i_b and i_c in the *abc* frame when the phase θ equals $\omega_s t$.

$$\begin{aligned} i_q &= \frac{2}{3}\frac{3}{2} I_m cos(\omega_s t - \theta) \\ &= I_m cos(\omega_s t - \theta) \end{aligned} \tag{4.12}$$

4.1.2 Voltage equations

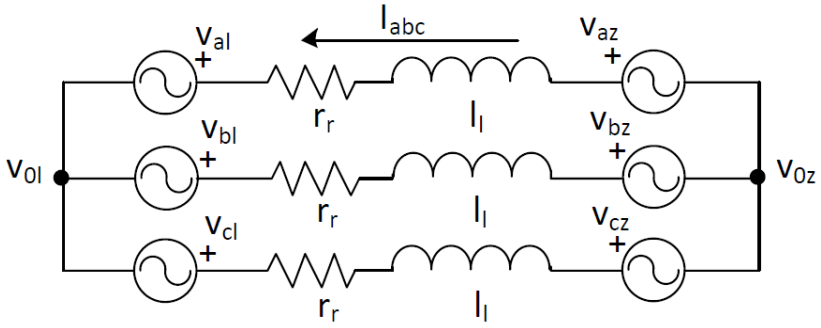

Figure 4.2: Equivalent model of the AC side of a Voltage Source Converter [1].

Using the equivalent model of the AC side of a Voltage Source Converter illustrated in figure 4.2, voltage equations can be defined as follows [1]:

In equation 4.13, v_{az}, v_{bz} and v_{cz} are the three-phase instantaneous voltages of the grid, v_{al}, v_{bl} and v_{cl} are the three-phase instantaneous voltages of the converter and i_a, i_b and i_c are the three-phase instantaneous currents. The voltage difference between the converter and the grid's neutral is $v_{0l} - v_{0z}$. All values are in the *abc* frame.

$$\begin{bmatrix} v_{az} \\ v_{bz} \\ v_{cz} \end{bmatrix} - \begin{bmatrix} v_{al} \\ v_{bl} \\ v_{cl} \end{bmatrix} - (v_{0l} - v_{0z}) \begin{bmatrix} 1 \\ 1 \\ 1 \end{bmatrix} = \begin{bmatrix} r_l & 0 & 0 \\ 0 & r_l & 0 \\ 0 & 0 & r_l \end{bmatrix} \begin{bmatrix} i_a \\ i_b \\ i_c \end{bmatrix} + \begin{bmatrix} l_l & 0 & 0 \\ 0 & l_l & 0 \\ 0 & 0 & l_l \end{bmatrix} \frac{d}{dt} \begin{bmatrix} i_a \\ i_b \\ i_c \end{bmatrix} \tag{4.13}$$

If no neutral conductor is present, equation 4.14 is true. When it is applied to three-wired balanced systems it results in equation 4.15.

$$v_{c0} - v_{z0} = \frac{1}{3} \begin{bmatrix} 1 & 1 & 1 \end{bmatrix} \cdot (v_z^{abc} - v_l^{abc}) \tag{4.14}$$

$$v_{c0} - v_{z0} = 0 \tag{4.15}$$

If the Park transformation is applied taking into account that $i_0 \equiv 0$, voltage equations result as seen in equation 4.16 below.

$$\begin{bmatrix} v_{zq} \\ v_{zd} \end{bmatrix} - \begin{bmatrix} v_{lq} \\ v_{lq} \end{bmatrix} = \begin{bmatrix} r_l & -l_l\omega_e \\ l_l\omega_e & r_l \end{bmatrix} \begin{bmatrix} i_q \\ i_d \end{bmatrix} + \begin{bmatrix} l_l & 0 \\ 0 & l_l \end{bmatrix} \frac{d}{dt} \begin{bmatrix} i_q \\ i_d \end{bmatrix} \tag{4.16}$$

4.1.3 Current Loop Control

By assuming $v_{zd} = 0$ in equation 4.16, voltage equations result as seen in equation 4.17 below.

$$\begin{bmatrix} v_{zq} \\ 0 \end{bmatrix} - \begin{bmatrix} v_{lq} \\ v_{lq} \end{bmatrix} = \begin{bmatrix} r_l & l_l\omega_e \\ -l_l\omega_e & r_l \end{bmatrix} \begin{bmatrix} i_q \\ i_d \end{bmatrix} + \begin{bmatrix} l_l & 0 \\ 0 & l_l \end{bmatrix} \frac{d}{dt} \begin{bmatrix} i_q \\ i_d \end{bmatrix} \tag{4.17}$$

A coupling between the q and d components of both voltages and current can be appreciated.

The purpose of the Current Loop Control (CLC) is to control that the current reaches the target value. Additionally, i_q and i_d are decoupled in order to avoid that altering one's value affects the other.

For decoupling the q and d components, equation 4.18 is used, where $\hat{v}_{lq}$ and $\hat{v}_{ld}$ represent the outputs of the current controllers and v_{lq} and v_{ld} the voltages to be applied by the converter.

$$\begin{bmatrix} v_{lq} \\ v_{ld} \end{bmatrix} = \begin{bmatrix} -\hat{v}_{lq} + v_{zq} - l_l\omega_e i_{ld} \\ -\hat{v}_{ld} + l_l\omega_e i_{lq} \end{bmatrix} \tag{4.18}$$

Substituting these in the voltage equations 4.17 results in equations 4.19 below.

$$\begin{bmatrix} \hat{v}_{lq} \\ \hat{v}_{ld} \end{bmatrix} = \begin{bmatrix} r_l & 0 \\ 0 & r_l \end{bmatrix} \begin{bmatrix} i_q \\ i_d \end{bmatrix} + \begin{bmatrix} l_l & 0 \\ 0 & l_l \end{bmatrix} \frac{d}{dt} \begin{bmatrix} i_q \\ i_d \end{bmatrix} \tag{4.19}$$

Which, after applying the Laplace transformation, define the transfer function between the controller voltages and converter currents as seen in equations 4.20 and 4.21 that follow.

$$\frac{\hat{v}_{lq}}{i_q(s)} = \frac{1}{l_l s + r_l} \tag{4.20}$$

$$\frac{\hat{v}_{ld}}{i_d(s)} = \frac{1}{l_l s + r_l} \tag{4.21}$$

By using Internal Model Control, the controller is designed in [1] resulting as follows:

$$G_{ciq}(s) = G_{cid}(s) = \frac{K_p s + K_i}{s} \tag{4.22}$$

Constants K_p and K_i in equation 4.22 can be calculated as seen in equations 4.23 and 4.24, where τ is the closed loop time constant of the electrical system, chosen considering the converter's physical restrictions.

$$K_p = \frac{l_l}{\tau} \tag{4.23}$$

$$K_i = \frac{r_l}{\tau} \tag{4.24}$$

The full implementation of the CLC is illustrated in figure 4.3.

Considering a base case limited to three seconds where the converter injects $i_q = 100[A]$ at the one second mark and $i_d = 100[A]$ at the two-second mark, the evolution of the currents' value varies depending on the presence or lack thereof the CLC.

The system's response when the decoupling is not implemented in the CLC can be appreciated in figure 4.4. The effect of one current's variation can be appreciated on the other at both instants in which either of them is injected.

If the same case is studied with the decoupling being implemented in the CLC, injection of i_q does not affect i_d and vice-versa. This can be appreciated in figure 4.5.

4.1.4 Phase Locked Loop

This V_d control method is a Phase Locked Loop (PLL) control method based on the one seen at [1, 24]

The PLL allows a synchronous relation between the converter and the grid by evening the frequencies, bringing the former's to the value of the latter. With it, the phase of the electrical grid is tracked and used in the Park transformation, since the $qd0$ reference frame used rotates to adjust to the grid angle.

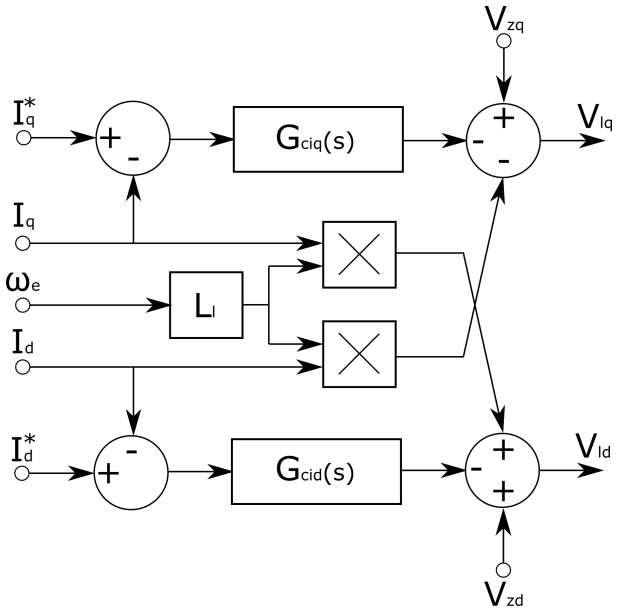

Figure 4.3: Block diagram of the Current Loop Control.

When the converter's phase matches that of the grid, the value of V_d in the *qd0* reference frame is zero. The phase locked loop controls the V_d voltage in order to bring it to this target value and, by doing so, matches the converter's phase with the grid's.

In order to analyze the response of the PLL controller, the angle error is assumed to be small, linearizing the system. This leads us to a second order system defined as seen in equation 4.25, with $\hat{\theta}(s)$ being the estimated grid angle and $\theta(s)$ the real one [1].

$$\frac{\hat{\theta}(s)}{\theta(s)} = \frac{2\xi\omega_n s + \omega_n^2}{s^2 + 2\xi\omega_n + \omega_n^2} \tag{4.25}$$

The PI controller inside the PLL control is defined as follows:

$$K_I = \frac{K_P}{\tau_{PLL}} \tag{4.26}$$

$$\begin{aligned} K_f(s) &= \frac{K_I + K_P \cdot s}{s} \\ &= \frac{\frac{K_p}{\tau_{PLL}} + K_P \cdot s}{s} \\ &= K_p \cdot \frac{\frac{1}{\tau_{PLL}} + s}{s} \end{aligned} \tag{4.27}$$

The controller parameters K_p and τ_{PLL} can be defined using equations 4.28 and 4.29 below. In these, ω_n is the natural frequency, E_m is the admitted peak voltage and ξ is the damping ratio [1].

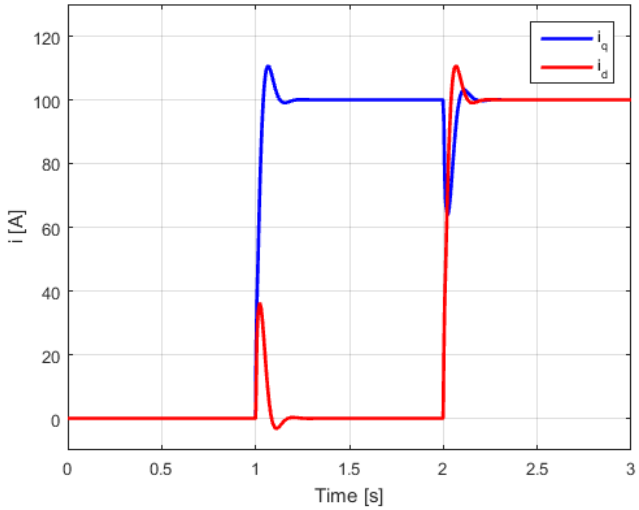

Figure 4.4: i_q and i_d response without the Current Loop Control.

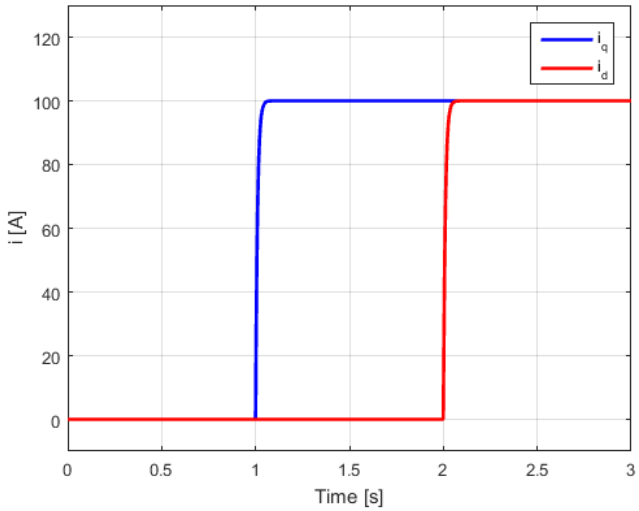

Figure 4.5: i_q and i_d response with the Current Loop Control.

$$\omega_n = \sqrt{\frac{K_p E_m}{\tau_{PLL}}} \tag{4.28}$$

$$\xi = \frac{\sqrt{\tau_{PLL} K_p E_m}}{2} \tag{4.29}$$

The Park Transformation must be applied to the grid voltage, since the PLL will be working with $qd0$ voltages. The PLL consists of the difference between a reference d voltage V_{dref} and the measured V_d filtered through a Proportional Integral control (PI). Its output, the grid frequency ω $[rad/sec]$, is then integrated in order to obtain the grid phase θ $[rad]$ which is later used for the Park transformation in order to feed V_d back to the system and close the loop.

The Phase Locked Loop requires three inputs; the grid's phase θ_{grid}, the target d voltage V_{dref} and the grid's voltage represented in the abc frame V_{abc}. Since the purpose of the PLL in this thesis is to match the converter's phase with that of the grid, the target d voltage value will be considered $V_{dref} = 0$.

Initially, the abc tension V_{abc} undergoes the Park Transformation seen in equation 4.1 taking into account that $\theta = \theta_{grid}$. The only component that interests the PLL is V_d; V_q and V_0 are terminated. V_d is then compared with the target d voltage V_{dref}.

Afterwards, the signal is processed by the Proportional Integral controller defined in equations 4.26-4.27. From this results the electrical frequency ω.

In order to obtain the phase value θ used for the Park transformation, the electrical frequency ω passes through an integrator. This phase θ is then fed back into the block corresponding to the Park transformation.

The implementation of the full block diagram is illustrated in figure 4.6.

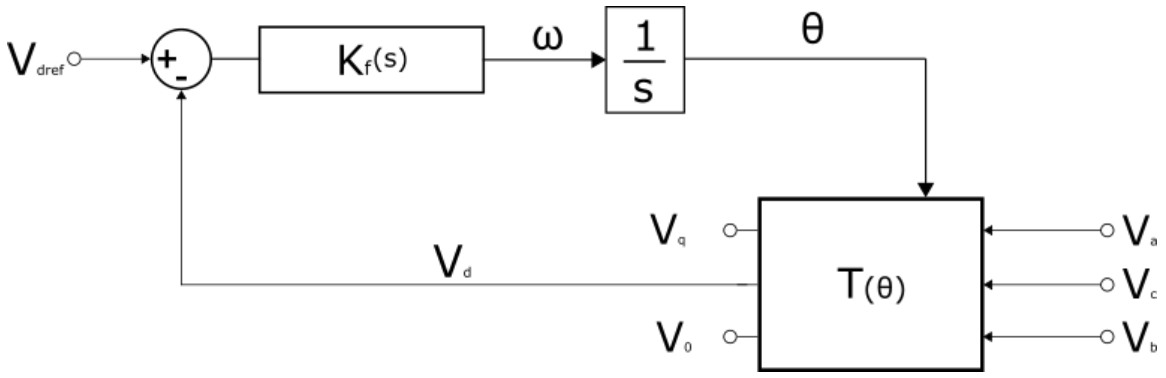

Figure 4.6: Block diagram of the Phase Locked Loop.

Thanks to the PLL controller the converter's frequency ends up being equal to that of the grid ω $[rad/s]$. In figure 4.7, the plot of $\Delta\omega = \omega_{converter} - 100\pi$ can be appreciated. It is noted that once stationary state is reached, $\Delta\omega$ does not equal 0 as it should; this is because the grid's frequency ω is not exactly the 100π $[rad/sec]$ used for the plot.

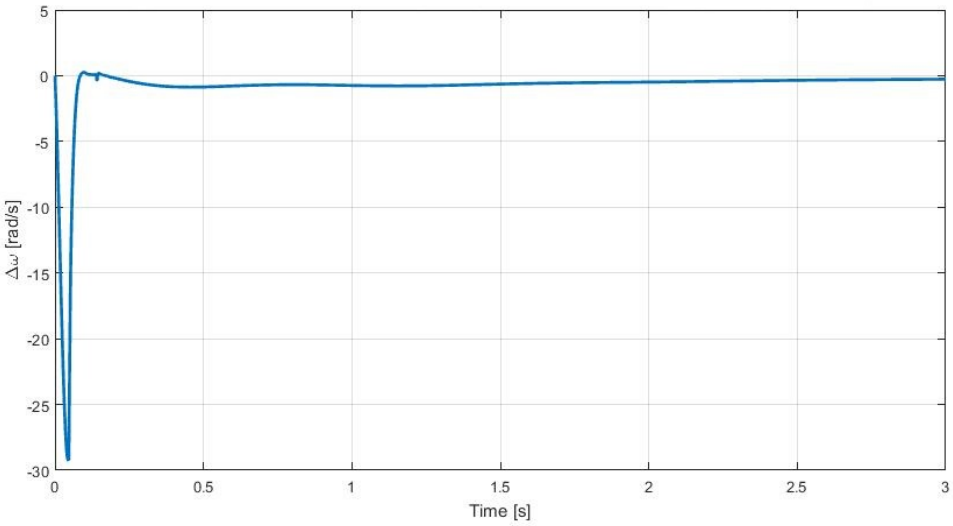

Figure 4.7: Evolution of $\Delta\omega$ through time as a consequence of the PLL.

4.1.5 Droop control

The droop control method allows for the control of active and reactive power injection to the grid by a Voltage Source Converter. For compensating the system's active and reactive power unbalances, the droop adjusts both frequency and amplitude of the output voltage [25, 26].

Conventional droop methods usually need the knowledge of some grid parameters in order to control active and reactive power flows independently [25].

Standard $P - f$ droop control is accomplished by means of equation 4.30 [27].

$$P_{conv} = (f_{ref} - f_{conv})K_{conv} + P_{ref} \tag{4.30}$$

Where P_{conv} is the power injected by the converter, P_{ref} is the real power set point at the nominal frequency, f_{ref} is the nominal frequency, f_{conv} is the converter's frequency and K_{conv} is the relation between the power injected per Hz of frequency deviation.

A schematic representation of the droop control used in this VSC converter model is shown in figure 4.8.

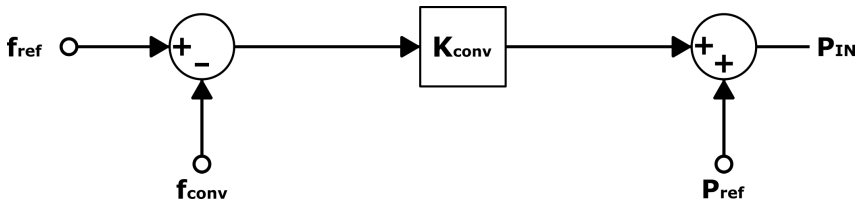

Figure 4.8: Block diagram of the converter's droop control.

4.2 Loads

Modelled as a three-phase passive linear branch, a resistance value R_{val} $[\Omega]$ is calculated as a function of the three-phase resistive load rated power P_{RL} $[MW]$ and the three-phase line-to-line voltage V_{RMS} $[kV]$ introduced. This is done following equation 4.31.

$$R_{val} = \frac{(V_{RMS})^2}{3 \cdot P_{RL}} \tag{4.31}$$

4.3 Generation

PV generation's implementation during the initial steady state analysis has been allowed because of the simplicity of the generation model used in MATPOWER [18].

Implementing Photo-voltaic (PV) generation in the dynamic model would have meant working on both the generation model for the PV generation and a different interface converter model that would be needed to connect the PV systems and the AC grid.

PV represents a minimal fraction of the studied case's total power generation and it is implemented in the $66kV$ part of the grid, which is not studied in the defined case. This is why it has been completely disregarded, leaving the HVDC connection, CCGT and traditional thermal power plants as energy sources.

The generation that derives from Combined Cycle Gas Turbine (CCGT) power plants and classical thermal power plants is modelled as the result of a synchronous machine's power generation. In order for it to function as intended, a turbine, an exciter and the frequency droop control method have been implemented.

4.3.1 Synchronous machine model

A synchronous machine's rotor generally has a field winding and at least one damper winding. Because of the rotor being magnetically asymmetrical, a change of variables does not benefit it. But applying the Park transformation explained in section 4.1.1 does benefit stator variables.

A two-pole, three-phase, wye-connected (Y), salient pole rotor synchronous machine like the one shown in figure 4.9 is considered. This type of generators are better suited for high speed steam and gas turbines typically used in thermal power plants.

The modelling here explains uses as a reference a machine functioning as a motor, assuming positive stator currents into the machine. At the end of this subsection, the changes needed to adapt the equations to the synchronous machine working as a generator (assuming positive stator currents out of the machine) are explained.

The stator windings are identical sinusoidally distributed windings. Displaced 120^o, they all have N_s equivalent turns and an r_s resistance.The rotor is equipped with four windings; a field winding fd with N_{fd} equivalent turns and a r_{fd} resistance and three damper windings kd, $kq1$ and $kq2$. All three damper windings have N_{kd}, N_{kq1} and N_{kq2} equivalent turns and r_{kd}, r_{kq1} and r_{kq2} resistances. The magnetic axis of the the damper windings $kq1$ and $kq2$ is displaced 90^o

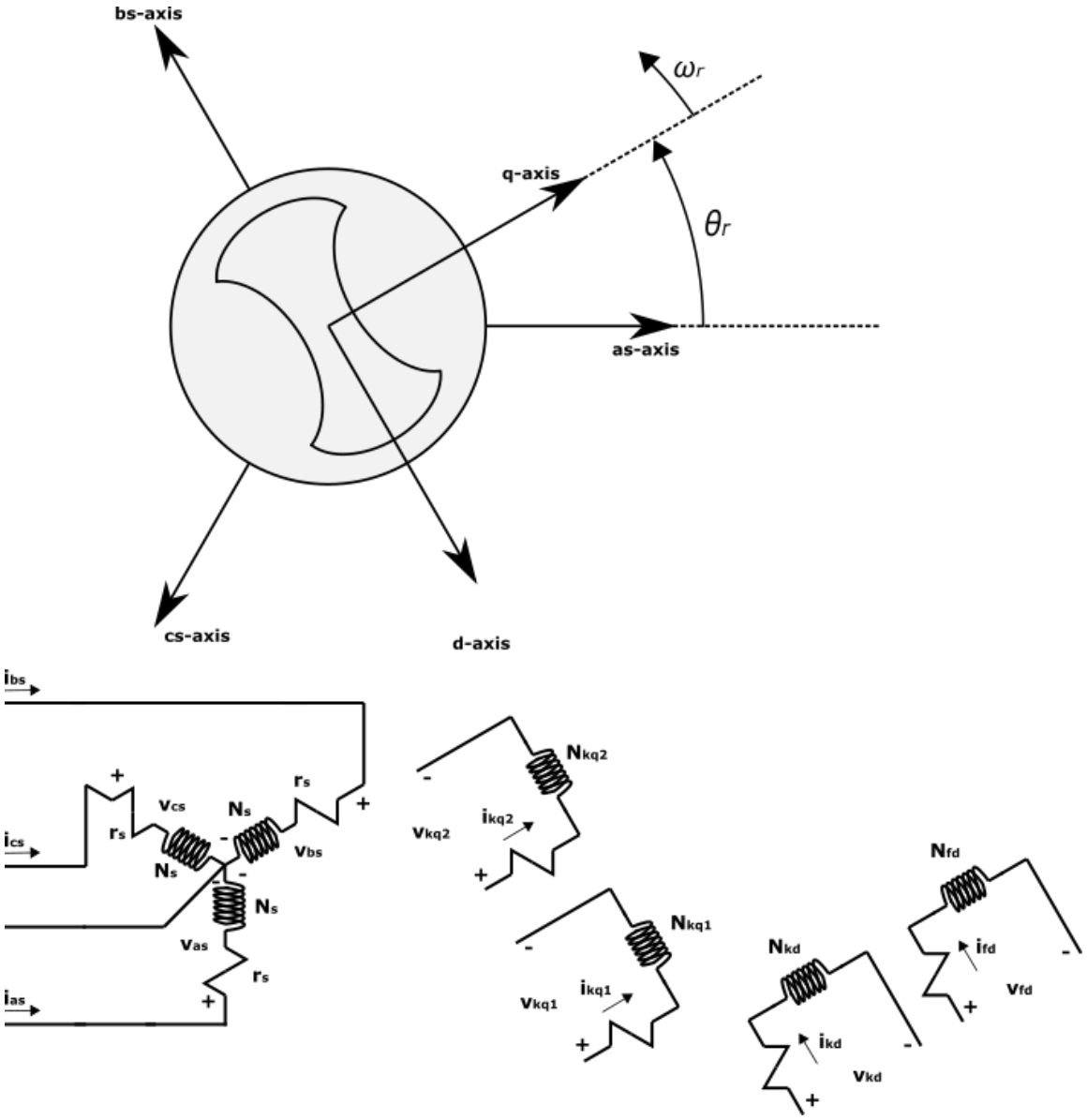

Figure 4.9: Two-pole, three-phase, wye-connected salient-pole synchronous machine.

ahead of the magnetic axes of the field winding fd and and the first damper winding kd [28]. In figure 4.9, *as*, *bs* and *cs* represent the magnetic axes tied to the stator windings [28].

The magnetic axes tied to the rotor windings, the quadrature axis *q-axis* and the direct axis *d-axis*, represent the magnetic axis of the $kq1$ and $kq2$ pair and the fd and kd pair respectively. Even if the damper windings kd, $kq1$ and $kq2$ are shown with the possibility of applying voltage, they actually are short-circuited windings that represent the paths for induced rotor currents [28].

Stator and rotor voltage equations are as seen in equations 4.32 and 4.33 [28].

$$\left[V_{abcs}\right] = \left[R_s\right]\left[I_{abcs}\right] + \frac{d}{dt}\left[\lambda_{abcs}\right] \tag{4.32}$$

$$\left[V_{qdr}\right] = \left[R_r\right]\left[I_{qdr}\right] + \frac{d}{dt}\left[\lambda_{qdr}\right] \tag{4.33}$$

If each component of the different matrices of equations 4.32 and 4.33 is expressed, equations 4.34 and 4.35 result.

$$\begin{bmatrix} v_{as} \\ v_{bs} \\ v_{cs} \end{bmatrix} = \begin{bmatrix} r_s & 0 & 0 \\ 0 & r_s & 0 \\ 0 & 0 & r_s \end{bmatrix} \begin{bmatrix} i_{as} \\ i_{bs} \\ i_{cs} \end{bmatrix} + \frac{d}{dt} \begin{bmatrix} \lambda_{as} \\ \lambda_{bs} \\ \lambda_{cs} \end{bmatrix} \tag{4.34}$$

$$\begin{bmatrix} v_{kq1} \\ v_{kq2} \\ v_{fd} \\ v_{kd} \end{bmatrix} = \begin{bmatrix} r_r & 0 & 0 & 0 \\ 0 & r_r & 0 & 0 \\ 0 & 0 & r_r & 0 \\ 0 & 0 & 0 & r_r \end{bmatrix} \begin{bmatrix} i_{kq1} \\ i_{kq2} \\ i_{fd} \\ i_{kd} \end{bmatrix} + \frac{d}{dt} \begin{bmatrix} \lambda_{kq1} \\ \lambda_{kq2} \\ \lambda_{fd} \\ \lambda_{kd} \end{bmatrix} \tag{4.35}$$

Where the flux linkage equations are as seen in equation 4.36 below [28].

$$\begin{bmatrix} \lambda_{as} \\ \lambda_{bs} \\ \lambda_{cs} \\ \lambda_{kq1} \\ \lambda_{kq2} \\ \lambda_{fd} \\ \lambda_{kd} \end{bmatrix} = \begin{bmatrix} \left[L_s\right] & \left[L_{sr}\right] \\ (\left[L_{sr}\right])^T & \left[L_r\right] \end{bmatrix} \begin{bmatrix} i_{as} \\ i_{bs} \\ i_{cs} \\ i_{kq1} \\ i_{kq2} \\ i_{fd} \\ i_{kd} \end{bmatrix} \tag{4.36}$$

Where L_s, L_{sr} and L_r are the different inductance matrices [23].

Electrical torque is ultimately tied to the voltage equations by means of equation 4.37 below.

$$\Gamma_e = \frac{P}{2}\left\{\tfrac{1}{2}(\left[I_{abcs}\right])^T \tfrac{\delta}{\delta\theta_r}\left[L_s\right]\left[I_{abcs}\right] + (\left[I_{abcs}\right])^T \tfrac{\delta}{\delta\theta_r}\left[L'_{sr}\right]\left[I'_{qdr}\right]\right\} \tag{4.37}$$

In equation 4.38 define the relation between the mechanical torque Γ_m, the electrical torque Γ_e and the rotor's speed ω_r. This in turn relates the turbine's torque and the machine's electrical

torque. Equation 4.38 is written taking generation action from the synchronous machine in to account. If the motor action reference used during the development of the equations explained in this section was followed, the signs of the torques Γ_m and Γ_e would have to be changed.

$$\Gamma_m - \Gamma_e = \tau \cdot \frac{d\omega_r}{dt} \tag{4.38}$$

Applying the Park transformation explained in section 4.1.1 to the synchronous machine allows us to eliminate the position-varying inductances in the voltage equations [28]. This is achieved by setting the speed of the reference frame equal to that of the rotor.

The resulting voltage equations are as follows:

$$v_{qs}^r = r_s i_{qs}^r + \omega_r \lambda_{ds}^r + \frac{d}{dt}\lambda_{qs}^r \tag{4.39}$$
$$v_{ds}^r = r_s i_{ds}^r - \omega_r \lambda_{qs}^r + \frac{d}{dt}\lambda_{ds}^r \tag{4.40}$$
$$v_{0s} = r_s i_{0s} + \frac{d}{dt}\lambda_{0s}^r \tag{4.41}$$
$$v_{kq1}^{'r} = r'_{kq1} i_{kq1}^{'r} + \frac{d}{dt}\lambda_{kq1}^{'r} \tag{4.42}$$
$$v_{kq2}^{'r} = r'_{kq2} i_{kq2}^{'r} + \frac{d}{dt}\lambda_{kq2}^{'r} \tag{4.43}$$
$$v_{fd}^{'r} = r'_{fd} i_{fd}^{'r} + \frac{d}{dt}\lambda_{fd}^{'r} \tag{4.44}$$
$$v_{kd}^{'r} = r'_{kd} i_{kd}^{'r} + \frac{d}{dt}\lambda_{kd}^{'r} \tag{4.45}$$

And the expressions for the flux linkages are as seen in equations 4.46-4.52 below.

$$\lambda_{qs}^r = L_{ls} i_{qs}^r + L_{mq}(i_{qs}^r + i_{kq1}^{'r} + i_{kq2}^{'r}) \tag{4.46}$$
$$\lambda_{ds}^r = L_{ls} i_{ds}^r + L_{md}(i_{ds}^r + i_{fd}^{'r} + i_{kd}^{'r}) \tag{4.47}$$
$$\lambda_{0s}^r = L_{ls} o_{0s} \tag{4.48}$$
$$\lambda_{kq1}^{'r} = L'_{lkq1} i_{kq1}^{'r} + L_{mq}(i_{qs}^r + i_{kq1}^{'r} + i_{kq2}^{'r}) \tag{4.49}$$
$$\lambda_{kq2}^{'r} = L'_{lkq2} i_{kq2}^{'r} + L_{mq}(i_{qs}^r + i_{kq1}^{'r} + i_{kq2}^{'r}) \tag{4.50}$$
$$\lambda_{fd}^{'r} = L'_{lfd} i_{fd}^{'r} + L_{md}(i_{ds}^r + i_{fd}^{'r} + i_{kd}^{'r}) \tag{4.51}$$
$$\lambda_{kd}^{'r} = L'_{lkd} i_{kd}^{'r} + L_{md}(i_{ds}^r + i_{fd}^{'r} + i_{kd}^{'r}) \tag{4.52}$$

These voltage and flux linkage equations suggest the equivalent circuit seen in figure 4.10.

When adapting the equations to generator action, positive stator currents out of the machine are considered, but the field and damper winding currents are still considered positive into the machine. In order to apply this, changing the sign of stator currents or its substitute variables.

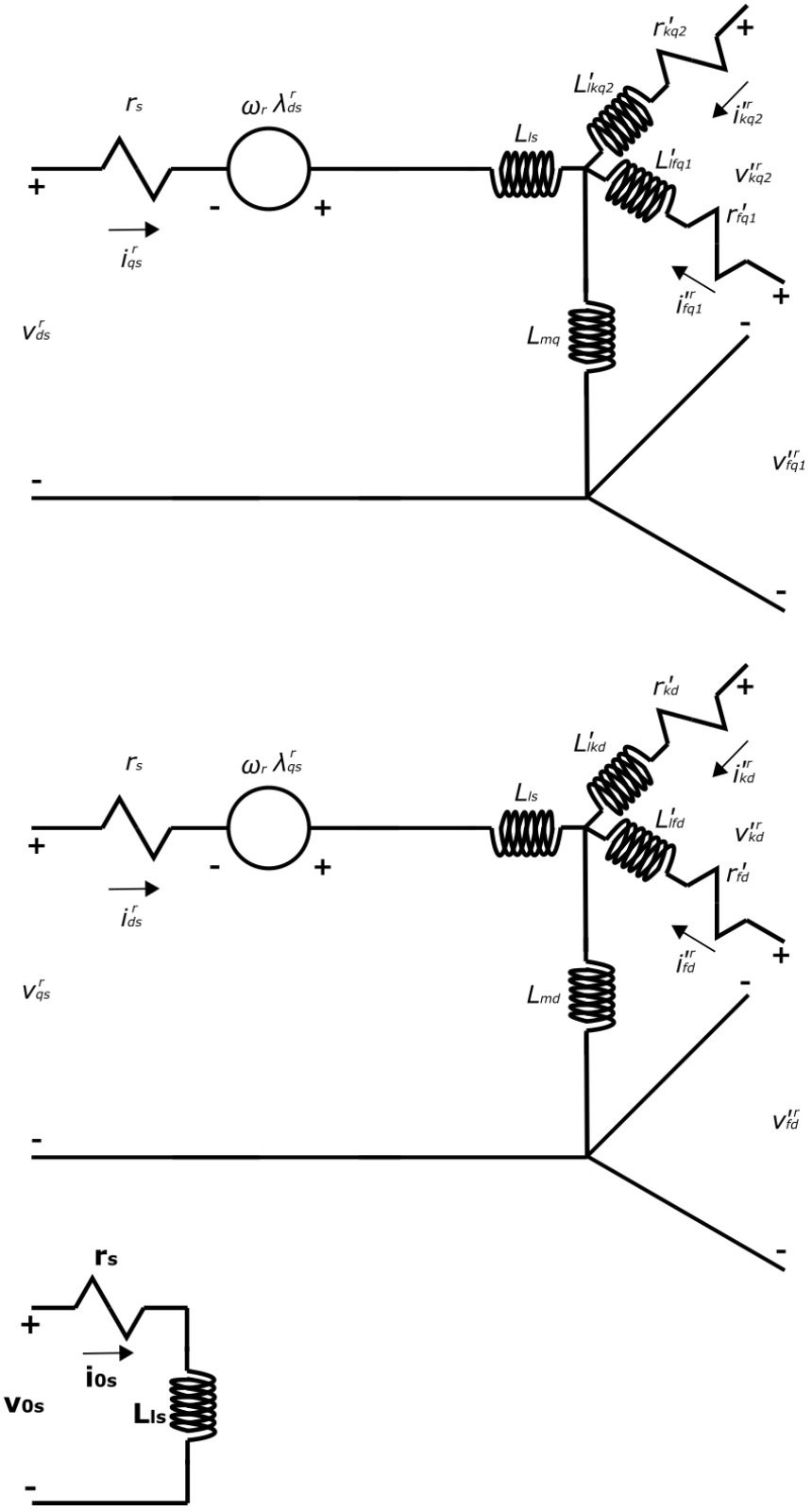

Figure 4.10: Equivalent circuits of the three-phase synchronous machine using Park's equations to fix the reference frame to the rotor.

4.3.2 Droop control

Just like in section 4.1.5, the generation also implements droop control. The only difference is that while the converter's droop control directly inputs the current value needed to feed the right amount of active power to the system, the generation's droop inputs the control valve flow area to the turbine model. Figure 4.11 shows a schematic of the generation's droop control.

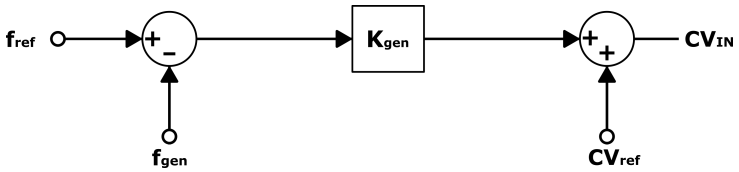

Figure 4.11: Schematic representation of generator's droop control's block diagram.

4.3.3 Turbine model

A graphical representation of the turbine modelled can be seen in figure 4.12. The steam coming from a boiler enters the cycle through the steam chest, its flow into a high pressure rotor HP managed via the control valve CV. The fluid is then reheated and directed to an intermediate pressure rotor IP. An intercept valve IV between the reheater and the intermediate pressure rotor facilitates the shutdown of the turbine in the case of a turbine trip. The fluid goes through a crossover that connects both the inlet and the exhaust piping before reaching one last low pressure rotor LP. All three rotors share a common shaft.

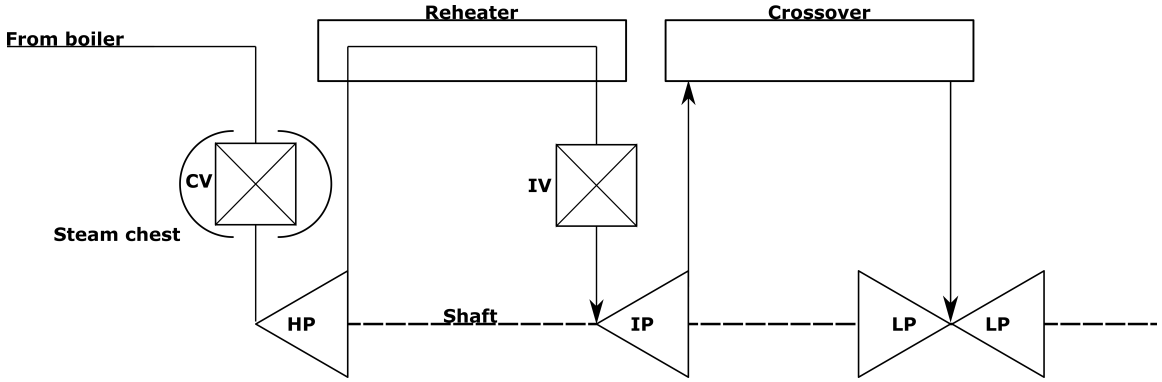

Figure 4.12: Schematic representation of the used turbine.

The turbine model is based on that seen in [23]. Given the control valve flow area C_V fed by the generator's droop control, it applies a transfer function as defined in figure 4.13.

In it T_1 represents the steam chest time constant, T_2 represents the reheater's time constant and T_3 represents the crossover piping's time constant. K_1, K_2 and K_3 represent the p.u. fractions of the flow, being the high pressure, the intermediate pressure and the low pressure respectively. As a result, the mechanical power in Per Unit is obtained.

All turbines used in this thesis have been considered equal, the values of their different constants listed in table 4.1. These values are based on those specified for a tandem-compound single-reheat turbine of fossil-fuelled units as sen in Sec. 9.2 of [23].

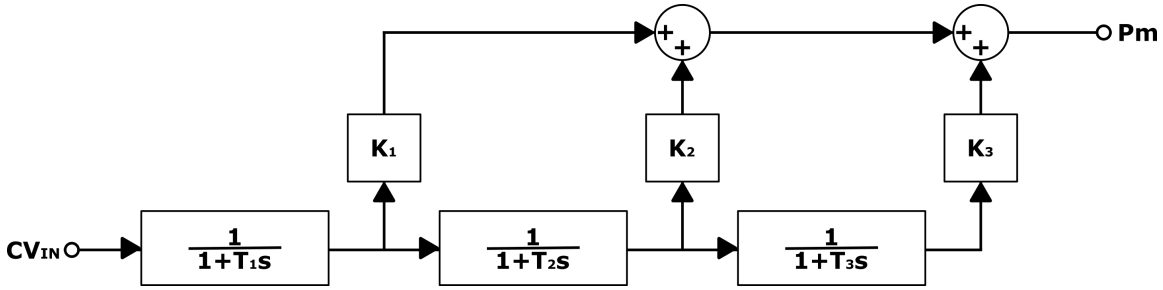

Figure 4.13: Schematic representation of the turbine model's block diagram function.

Table 4.1: Values of τ_1, τ_2, τ_3, K_1, K_2 and K_3 for all turbines.

Constant	Value
τ_1 $[s]$	0.3
τ_2 $[s]$	7.0
τ_3 $[s]$	0.5
K_1 $[p.u.]$	0.3
K_2 $[p.u.]$	0.3
K_3 $[p.u.]$	0.4

4.3.4 Exciter model

A simplified version of the standard AC4A (Alternator Supplied Rectifier Exciter #4) IEEE® type exciter model is used [23]. Figure 4.14 represents the simplified exciter's block diagram.

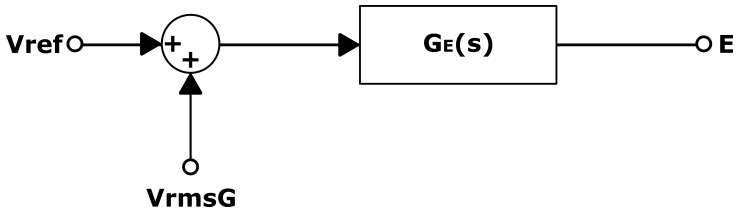

Figure 4.14: Schematic representation of the exciter's block diagram.

The regulator's transfer function $G_E(s)$, with a gain K_r and a time constant τ_r is defined as seen in equation 4.53 model below. The time constant τ_r is associated with the regulator and the firing of thyristors, while K_r represents the overall gain.

$$G_E(s) = \frac{K_r}{1 + \tau_r s} \tag{4.53}$$

The regulator constants of the exciter have been defined as $K_r = 200$ and $\tau_r = 0.04$ [23]. If these are applied to equation 4.53, the following exciter transfer function results:

$$G_E(s) = \frac{200}{1 + 0.04s} \tag{4.54}$$

4.3.5 Transformer model

An ideal three-phase two-winding transformer is represented by the ideal three-phase two-winding model. Only the positive leakage reactance is considered, while the losses are neglected.

Figure 4.15 illustrates the model, where S_N is the rated power, V_1 and V_2 are the voltages on each side and L_{lr} is the positive sequence leakage reactance..

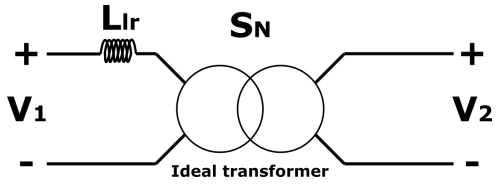

Figure 4.15: Schematic representation of the transformer model.

Chapter 5

Dynamic Analysis: Case, simulation and results

In this chapter the case is defined for the dynamic model and the results of the simulation are given. Even if the basis is the same as the one used for the steady state analysis, a few details differ and the differences in implementation force slight changes.

5.1 Case

Transmission lines for the dynamic case are defined as the same used for the steady state case. The details can be seen in 3.1.1. Loads for the dynamic case are also the same used for the steady state case. The details and values can be seen in section 3.1.2.

Three main blocks are considered when defining the case; the grid, the converter and the generation. The grid is characterized by a nominal frequency of 50 Hz and a 220 kV peak voltage. The HVDC connection has a rated power of 400 MW, and the different synchronous generators at *SONREUS4*, *CASTRES7* and *ESMURTERAR9*, with a shared inertia constant of 3.84 s and a common RMS rated voltage of 11.5 kV, each present rated powers of 630, 430 and 530 MW respectively. Each generator's droop constant K_{gen} is equal to 20, representing a 20% of nominal power per Hz affected; individual values taking this into account have been calculated for each generator. All related constants and values are listed in table 5.1.

The transformers that connect the synchronous generators and the grid are defined with a three-phase apparent power rating equal to the rated power S_N of the machine they are connected to and a base operation frequency of 50Hz. The winding on the generator's side of the transformer has a root mean square (RMS) voltage rating of 11.5kV, in concordance with that of the synchronous machine's output. The winding on the grid's side of the transformer has a RMS voltage rating of 220kV, in concordance with that of the grid. The positive sequence leakage reactance's value has been set at 0.1p.u. with the synchronous machine's RMS voltage as the rated voltage used for obtaining its reduced value.

Table 5.1: List of the different variables that define the case, including the variable name, its symbol used during the development of the model, its value and the corresponding units.

Block	Variable	Symbol	Value	Unit
Grid	Nominal frequency	f_{grid}	50	Hz
	Peak voltage	V_{Ngrid}	220	kV
Converter	Rated power	P_{Nconv}	400	MW
	Droop gain	K_{conv}	200	MW/Hz
	Power at 50Hz	$P_{refconv}$	242	MW
	Converter's internal resistance	r_r	0.1	ohms
	Converters internal inductance	l_l	0.025	H
	CLC time constant	τ	0.002	s
	Natural frequency	ω_n	100π	rad/s
	Damp ratio	ξ	0.7	-
Generation	SONREUS4 rated power	P_{g4}	630	MW
	CASTRES7 rated power	P_{g7}	430	MW
	ESMURTERAR9 rated power	P_{g9}	530	MW
	SONREUS4 droop gain	K'_{gen4}	126	MW/Hz
	CASTRES7 droop gain	K'_{gen7}	86	MW/Hz
	ESMURTERAR9 droop gain	K'_{gen9}	106	MW/Hz
	Inertia constant	H	3.84	s
	RMS Rated voltage	V_n	11.5	kV
	SONREUS4 Cv at 50Hz	C_{vref4}	0.236	p.u.
	CASTRES7 Cv at 50Hz	C_{vref7}	0.157	p.u.
	ESMURTERAR9 Cv at 50Hz	C_{vref9}	0.459	p.u.

5.2 Simulation and results

During the simulation, a fault is forced at the five seconds mark once steady state has been reached. When the fault happens, the synchronous machine functioning as a generator at the bus *ESMURTERAR9* is suddenly disconnected from the grid.

5.2.1 Bus voltage

The different bus voltages measured during the initial steady state of the grid are shown in table 5.2. V refers to the voltages obtained from the PSCAD 4.6 EDU simulation, while V_{ss} refers to the voltages obtained from the Matlab®2015b simulation.

When looking at the table 5.2, the main difference that arises between both simulations is the voltage on generating buses. This is explained by the fact that during the steady state analysis generating buses are defined as PV, meaning that their voltage magnitude is fix at the rated value. The bus *ESP1*, where the High Voltage Direct Current (HVDC) connection is found, is defined as a PQ bus and as a results its voltage magnitude is not fix to the rated value. This is not the case for the dynamic simulation, where voltage is not controlled on generating buses and as a consequence it differs from the rated power.

Table 5.2: Voltages V and V_{ss} of each bus in p.u..

Bus index	V [p.u.]	V_{ss} [p.u.]
ESP1	1.0005	1.005
STPON2	1.0000	1.004
VURG3	0.9968	1.001
SONREUS4	0.9955	1.000
LLUBI5	0.9927	0.998
SORLAND6	0.9918	0.998
CASTRES7	0.9913	1.000
BESSONS8	0.9909	0.997
ESMURTERAR9	0.9950	1.000
STMARTI10	0.9950	1.000

Once this is taken into account, the values are relatively similar; the voltage drops that happen between neighbouring buses remain the same among both simulations, but the values in the steady state simulation are slightly higher than their counterparts from the dynamic simulation because the fixed voltage at generating buses forces these values to rise.

5.2.2 Power flows

Figure 5.1 shows a schematic representation of the power flow obtained by the dynamic simulation done with PSCAD.

If figures 3.2 and 5.1 are compared, light differences in active power flow are noticed. There are three main reasons for these:

1. *The PV generation.* Since Photo-voltaic generation was not included in the dynamic analysis, buses with PV generation fall short of a few MW which need to be fed by either the HVDC connection or the synchronous generators.

2. *Droop constants, frequency and power variations.* Even if the synchronous generator's droop constants were defined in order to supply the same power than the steady-state analysis, the converter's was changed in order to rise the working frequency to $50Hz$. This means that in the dynamic analysis the converter is feeding slightly more power than it does in the steady-state analysis. This alters the power flow results.

3. *The load model.* The load model is based on a rated resistance value that at the corresponding rated voltage value consumes the specified active power, and this translates into voltage variations making the power consumption at the different loads vary. Since buses in steady state analysis are defined as PQ buses with a constant active and reactive power consumption, these loads remain unaffected by voltage variations.

In conclusion, the active power flow was as expected. The differences between the dynamic and the steady-state analysis are small and clearly tied to the aforementioned conditions, meaning that in regards to active power flow the dynamic model behaves as expected.

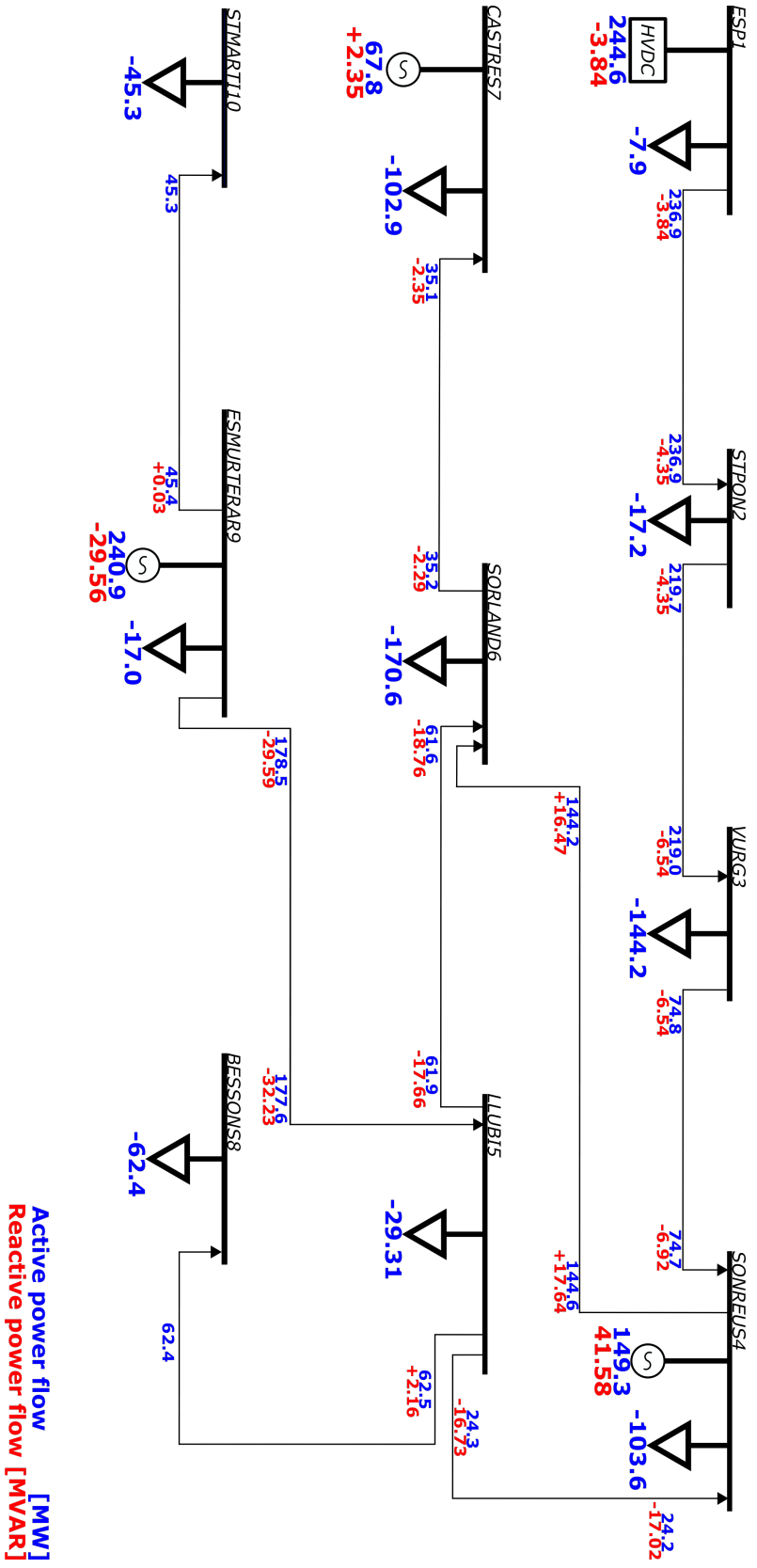

Figure 5.1: Power flow diagram for the peak demand case before the fault once steady state has been reached representing the values obtained via the PSCAD simulation.

By comparing figures 3.2 and 5.1, notable reactive power flow differences can be appreciated. The difference between each generator's power factors in each simulation is not negligible.

The main reason for these differences lays upon the type of buses generating buses are defined as in the steady state simulation and the control systems used for the generation in the dynamic model.

In the steady state simulation generating buses are defined as PV buses with a fix active power injection and a fix voltage equal to the rated one ($220kV$ in the studied case). For this to be implemented in the dynamic simulation, voltage control based on reactive power injection would have to be implemented.

In the dynamic simulation, voltage is not controlled on generating buses; when this is tied to the reactive-power based voltage control systems, the reason for the reactive power flow differences seen between both simulations becomes clear.

The reactive power situation can be explained, arguing that the lack of voltage control makes the constant power factor slightly difficult. This has been assumed for the steady state simulation but the dynamic would have needed the aforementioned control, so this might be a reason for differences.

5.2.3 VSC not supporting the grid frequency

When the converter does not provide frequency support it behaves as a constant power injection at *ESP1*. As a result, when the fault occurs its injected power does not vary. This lack of response to the system's fault translates into the generators at buses *SONREUS4* and *CASTRES7* being in charge of feeding the system with the power that was once fed by the generator at the bus *ESMURTERAR9*.

The consequences of the fault in regards to the power supplied by each generator can be appreciated in figure 5.2 below. *Pg4*, *Pg7* and *Pg9* represent the power generated at buses *SONREUS4*, *CASTRES7* and *ESMURTERAR9* respectively, while *PgC* represents the power injected at the bus *ESP1* by the VSC without droop control.

The generators at *SONREUS4* and *CASTRES7* are in charge of feeding the lost power. After the fault these are generating, in addition to what they were injecting into the system initially, 141.52 MW and 96.89 MW respectively. The sum of these power injection increases represents the 238.41 MW that are suddenly lost because of the fault at *ESMURTERAR9*.

The consequences of the fault in regards to the frequency of the remaining functioning generators at *SONREUS4* and *CASTRES7* can be appreciated in figure 5.3 below. In it, *f4* and *f7* represent the frequency of the synchronous machines functioning as generators at buses *SONREUS4* and *CASTRES7*.

Once steady state is reached, the frequencies of the generators at *SONREUS4* and *CASTRES7* are equal both before and after the fault. Their value varies from $49.9830Hz$ to $49.4182Hz$, which represents a $0.5648Hz$ drop.

The initial drop in frequency for the generators at buses *SONREUS4* and *CASTRES7* reach the $48.4229Hz$ and $48.4296Hz$ marks respectively, representing a $1.5532Hz$ and $1.5534Hz$ drop for each.

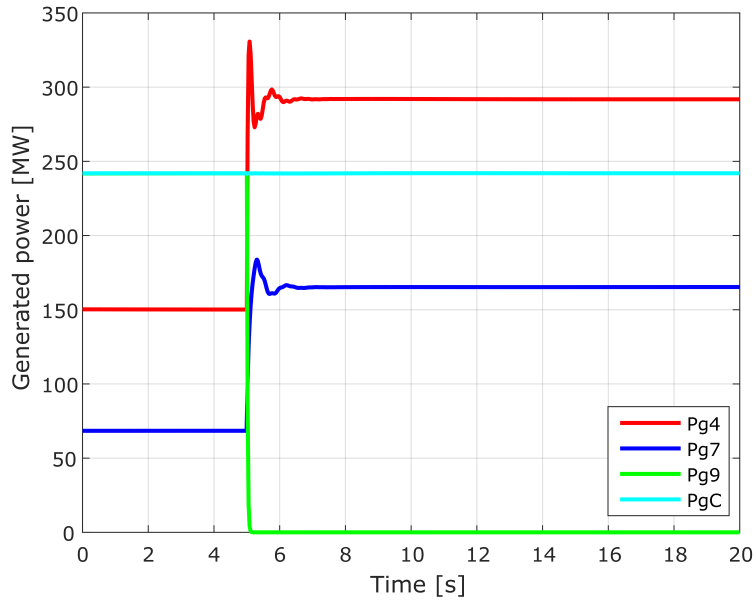

Figure 5.2: Plot of the power supplied by each generator versus time during the fault without frequency support.

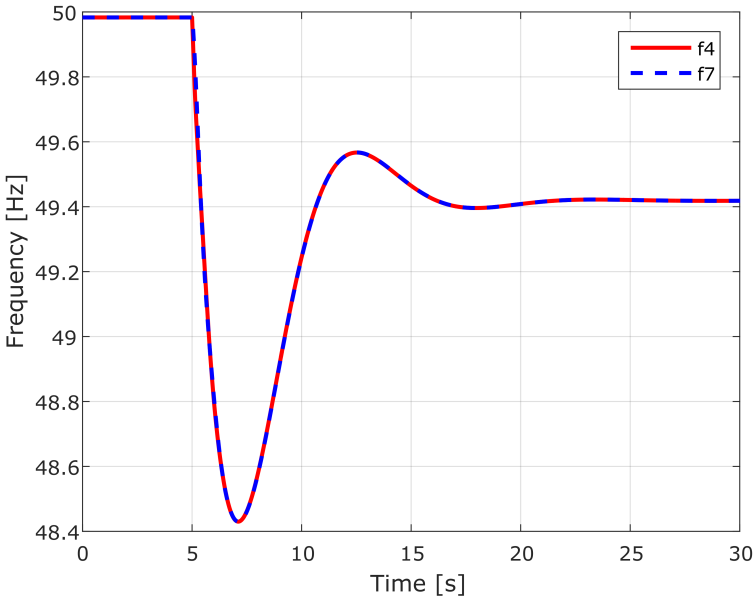

Figure 5.3: Plot of the different frequencies versus time during the fault without frequency support.

5.2.4 VSC supporting the grid frequency

When the converter functions with the droop control, the power it injects is related to the grid frequency it reads from the Phase Locked Loop (PLL). As a result, when the fault occurs its injected power varies, sharing the load with the generators at buses *SONREUS4* and *CASTRES7*.

This response to the system's fault translates into the generators at buses *SONREUS4* and *CASTRES7* not being solely in charge of feeding the system with the power that was once fed by the generator at the bus *ESMURTERAR9*, since the Voltage Source Converter can now inject power if needed.

The consequences of the fault in regards to the power supplied by each generator can be appreciated in figure 5.2 below. In it, *Pg4*, *Pg7* and *Pg9* represent the power generated at buses *SONREUS4*, *CASTRES7* and *ESMURTERAR9* respectively, while *PgC* represents the power injected at the bus *ESP1* by the VSC.

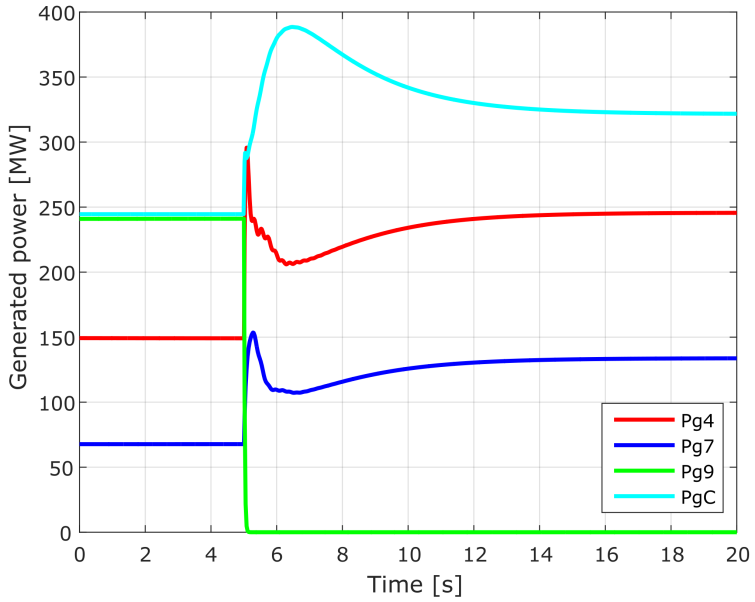

Figure 5.4: Plot of the power supplied by each generator versus time during the fault with frequency support.

The power injected by the converter undergoes a 77.21 *MW* increase, while the generators at *SONREUS4* and *CASTRES7* are feeding, in addition to what they were injecting into the system initially, 96.33 *MW* and 66 *MW* respectively.

The sum of these power injection increases represents the 239.54 *MW* that are suddenly lost because of the fault at *ESMURTERAR9*.

The consequences of the fault in regards to the frequency of the remaining functioning generators at *SONREUS4* and *CASTRES7* can be appreciated in figure 5.5 below. In it, *f4* and *f7* represent the frequency of the synchronous machines functioning as generators at buses *SONREUS4* and *CASTRES7*.

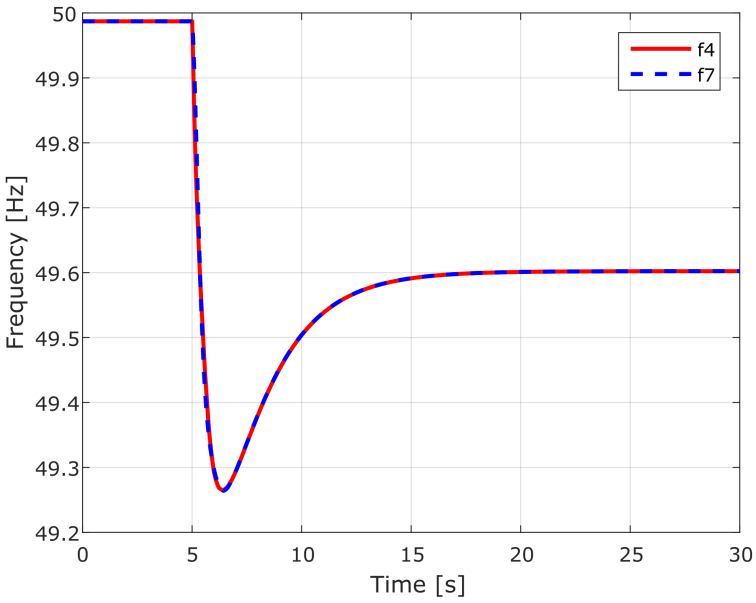

Figure 5.5: Plot of the different frequencies versus time during the fault with frequency support.

Once steady state is reached, the frequencies of the generators at *SONREUS4* and *CASTRES7* are equal both before and after the fault. Their value varies from 49.9871Hz to 49.6022Hz, which represents a 0.3849Hz drop.

The initial drop in frequency for the generators at buses *SONREUS4* and *CASTRES7* reach the 49.2651Hz and 49.2641Hz marks respectively, representing a 0.7220Hz and 0.7230Hz drop for each.

5.2.5 Analysis of the different reactions to the fault

Once steady state is reached, the frequency drop is larger on the model where the Voltage Source Converter (VSC) is not supporting the grid's frequency.

Without the frequency support, the grid's frequency drops to a minimum value of 48.4229[Hz] before reaching its steady state value of 49.4182[Hz]. This is particularly problematic because a frequency drop of such magnitude can have negative effects on the grid, making possible the need for load shedding in order to reduce the system's stress and bring the frequency back to a value closer to the rated one.

When the frequency support is introduced, the grid's frequency initial drop is drastically reduced, reaching a minimum value of 49.2641[Hz] before stabilizing at its steady state value of 49.6022[Hz].

Figure 5.6 compares the evolution of both frequencies in order to better illustrate the effect the converter's frequency support has on the system's response. In it, f_s represents the frequency of the grid with frequency support from the VSC and f_{sn} represents the frequency of the grid where the converter is not supporting the grid's frequency.

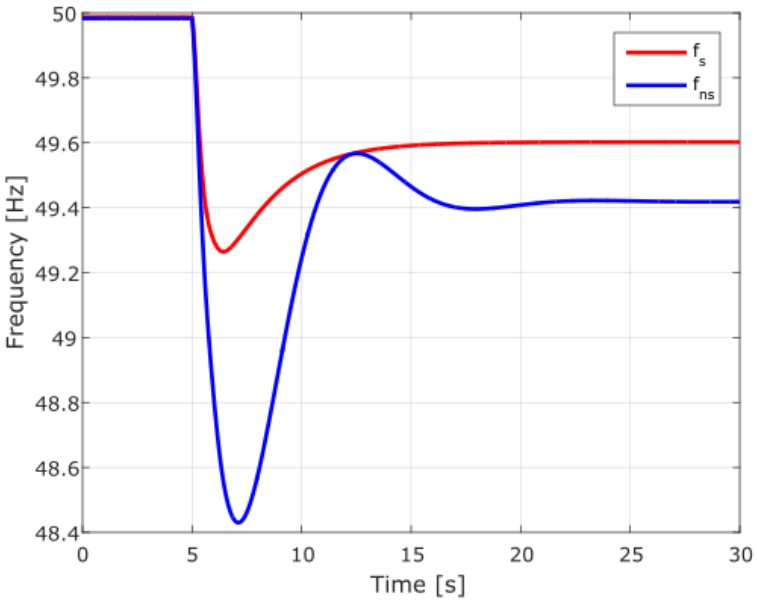

Figure 5.6: Plot of f_s and f_{sn} vs time.

When the converter is able to support the grid's frequency by injecting active power, the generators in buses *SONREUS4* and *CASTRES7* are subject to less stress from the grid, since they do not have to cover the sudden demand on their own. This can be appreciated in table 5.3.

The difference between the active power fed before and after the fault by each bus (*SONREUS4*, *CASTRES7* and *ESP1*) is illustrated in figures 5.7, 5.8 and 5.9.

Table 5.3: Power share of the fault's load covered by each generator depending on the presence or lack of grid frequency support in %.

Bus index	**f support**	**No f support**
ESP1	32.23%	00.00%
SONREUS4	40.21%	59.36%
CASTRES7	27.56%	40.64%

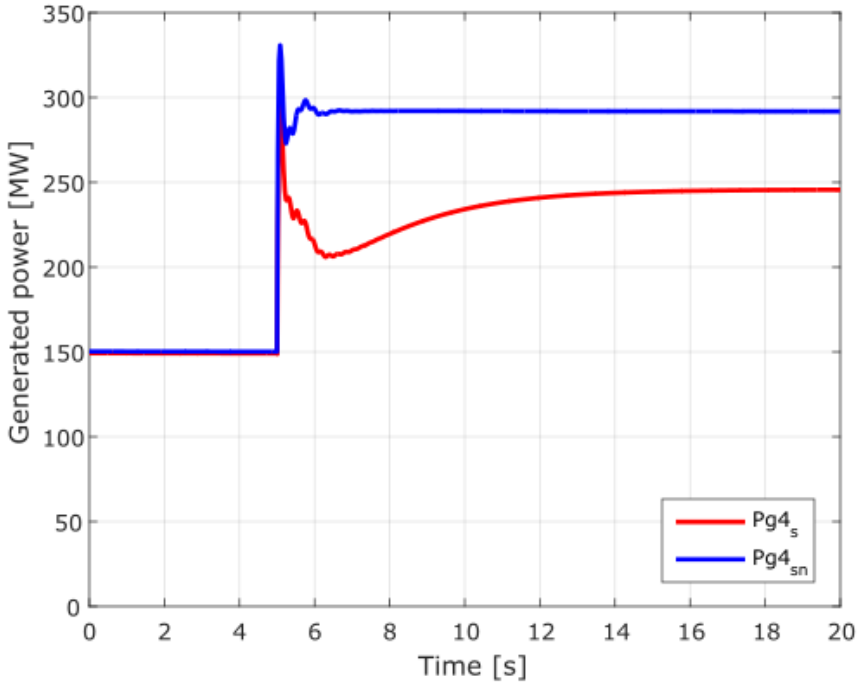

Figure 5.7: Plot of $Pg4_s$ and $Pg4_{sn}$ vs time.

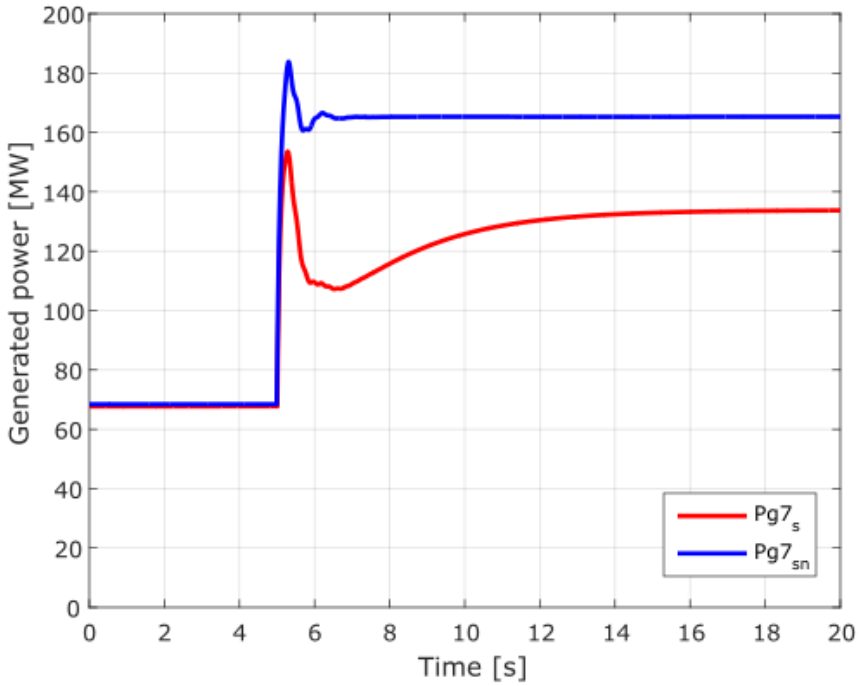

Figure 5.8: Plot of $Pg7_s$ and $Pg7_{sn}$ vs time.

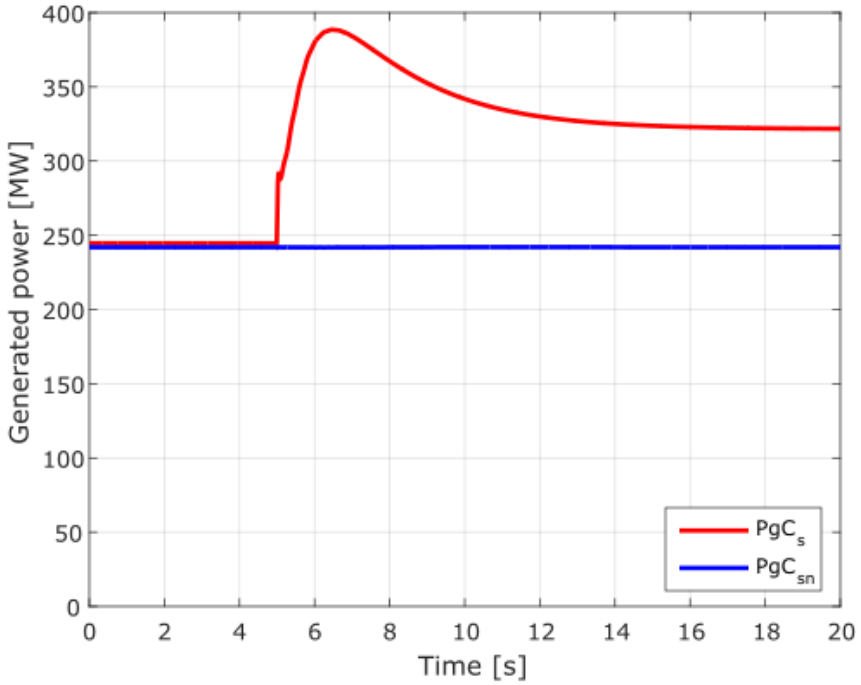

Figure 5.9: Plot of PgC_s and PgC_{sn} vs time.

Chapter 6

Conclusions

6.1 Consequences for insular power systems

As it has been explained in 1.1.3, grid frequency stability and general reliability of insular power systems is an issue heavily influenced by the limitations of isolated systems like islands in regards to the magnitude of power generation.

If one generator of the system were to cover most of the demand's power supply, the system would face grid security issues in front of the possibility of a fault like the one described in this thesis. This means that generators in isolated power systems like insular grids must have lower capabilities and share the burden of feeding the grid between them. This is done even when doing so translates into distribution systems with heavy transmission losses or generators functioning on suboptimal working points.

This is why the initial steady state analysis of the modelled grid was done using MatLab® 2015b. This analysis gave valuable information in regards to the system's power flow and its losses. It was possible to check that no part of the system was overburdened, that voltage levels remained between acceptable limits and that no transmission lines were overloaded.

Such less powerful systems generally present issues with frequency stability, since their inertia is sometimes not enough to guarantee the quality standards required of the grid, especially during unexpected transitions and faults. The dynamic analysis of the grid done via PSCAD 4.6 was performed in order to check the effects of frequency support on grid with such characteristics.

The results show the frequency support's positive effect on the grid. Frequency support from HVDC connections and their converter substations helps reduce the negative effects that contingencies like sudden changes in loads or generation faults have on the grid's frequency.

Another issue that arises from insular systems is their dependence on fossil fuel imports, as explained on 1.1.2. HVDC connections like the one studied in this thesis help mitigate these issues while at the same time reducing the environmental impact of energy consumption in insular systems.

Acknowledgements

En primer lugar me gustaría agradecer a Oriol por la oportunidad de llevar a cabo este trabajo de fin de grado. También es imprescindible agradecer la ayuda prestada en todo momento por Carlos, este trabajo no habría podido ser el mismo sin sus consejos, su experiencia y su apoyo; no hay palabras suficientes para representar lo que ha significado su ayuda. Quiero también agradecer a Marc y a toda la gente del CITCEA con la que a lo largo de estos meses he compartido tanto tiempo por su compañía.

En segundo lugar, quiero agradecer el inmesurable apoyo recibido por mi familia desde que empecé el grado, en especial a mis hermanos Agustín, Tomás y Lourdes, mis padres Ángeles y Andrés, mis abuelos Francisco Javier y Alicia y mi tía Isabel. Se agradece también el apoyo de todos los amigos de familia que desde la perspectiva que otorga la experiencia me han aconsejado durante todos estos años. Sin la presencia y el cariño de estas personas en la distancia no me hubiese sido posible llegar a dónde estoy hoy.

Por último, me gustaría agradecer la compañía de toda la gente que a lo largo de estos años he tenido la suerte de compartir esta época. Amigos de Mallorca, compañeros de clase, proyectos, estudio y también festejos en la ETSEIB, mentores del Aula Lliure y compañeros de piso pero, por encima de todo eso, compañeros de una etapa de mi vida que recordaré con gusto gracias a ellos.

Appendix A

Appendix

A Environmental impact

A.1 Insular grids and sustainability

Insular electrical power systems present a series of characteristics that distinguish their environmental impact from standard grids.

This section focuses on both how insular power systems behave in regards to CO_2 emissions (direct impact) and how complications arise when trying to tackle such an issue via the implementation of renewable energy sources.

Insular electrical grids are isolated power systems. Such systems, characterized by a low inertia, strongly require the one provided by traditional generators. Even if CO_2 emissions are lower with technologies like CCGT, fossil fuel generation contributes to global warming and climate change.

In the case of insular electrical power systems, the environmental effects are aggravated by a series of factors tied to their isolation and economy.

To the emissions caused by fossil fuel burning it is important to also add those caused by the transport of the different fuels to the island. Fossil fuel generation usually represents most if not all of the generation of an island, so this is not a negligible source of CO_2.

Grid quality should also be factored in when talking about the CO_2 emissions of insular systems. Generally, generating facilities in insular systems are old, relatively outdated when compared to more modern, efficient facilities.

Transmission losses are also another point to focus on when talking about the lack of efficiency of insular grids. Most insular systems are islands and these tend to rely heavily on tourism; this means that placing power plants close to where power is consumed is not an option, so transmission losses are higher than usual. The Majorcan grid is a clear example of this, with one of its stations with the highest rated power (Es Murterar, 530MW) is placed in a relatively far and isolated bus of the grid.

The dependency on fossil fuel imports and its effects on the environment call for a solution that is extremely common nowadays; the implementation of clean, renewable energy sources in

the power system. This would be a possible solution for insular grids if not for their security and stability issues; voltage and frequency deviations are quite problematic due to the insular systems' characteristically low inertia.

Renewable energy sources like Photo-voltaic (PV) and wind generation both generate no carbon emissions once they are functioning, but they are also unreliable and intermittent. This means that they cannot provide the inertia these fragile grids need; in fact, they may even worsen the situation of these issues.

A.2 Environmental Impact of HVDC transmissions

Even if it cannot be stated that DC transmission installations are more harmful to the environment than their AC counterpart, there are some aspects that must be considered when studying their impact on nature.

One of the main uses of HVDC transmissions are long distance connections through large bodies of water. This means that these cables need to lay on the seabed, which in turn requires excavations so that trenches for the cables can be made. This procedures can have a substantial impact on marine ecosystems.

The path followed by the cable needs to adhere to certain limitations:

1. *Avoid or minimize disruption of current activities in the affected areas.* Fishing or harvesting are two of the main activities that can be affected by these practices.
2. *Respecting wildlife.* If the optimal route for a cable to be laid on crosses areas where endangered species are located, alternative paths must be studied and followed. Even if the effect on marine wildlife must be minimized, recovery of submarine vegetation is usually not a problem even if it may take a year for it to get back to its original state.

In line with the fuel import dependency case of insular power systems, HVDC cable laying processes require the use of large ships; these CO_2 emissions cannot be neglected.

Also, efficiency is a key aspect of sustainability. Environmentally, the impact of energy generation is reduced if less power is consumed; this means that if less power is lost in transmission, less energy needs to be produced and as such CO_2 emissions and waste are reduced.

Even if High Voltage Direct Current transmission lines suffer less losses per distance than High Voltage Alternate Current connections, the efficiency of HVDC connections depends largely on the converter substations. This is where the concept of break-even distance is introduced; for an HVDC connection to be more efficient than its alternate current counterpart, the transmission has to be long enough so that AC losses are higher than those of the converter substations.

B Budget

B.1 Labour costs

Labour costs are divided depending on the type of work performed. Costs vary among them depending on the type of work and the specialization and information needed to perform such

task.

The details are as follows:

1. *Research.* This includes the hours dedicated to the gathering of information concerning the state of the art, the situation of insular grids and details on various of the models included. A cost of 12 €/ho has been considered because some previous knowledge is needed in order to know what type of documentation to look for and the interpretation needed after reading.

2. *Modelling.* This includes the hours dedicated to the mathematical modelling and the implementation of the models in the different software used during the development of this thesis. A cost of 24 €/h has been considered because of the technical and theoretical knowledge needed to design and implement the various models.

3. *Simulation.* This includes the hours dedicated to running the simulations and making sure that they function as they should during the development of this thesis. A cost of 6 €/h has been considered because during the time that simulations are running it is possible to multitask, allowing for *Research* and *Writing* to be done while the software runs the various simulations on the background.

4. *Analysis.* This includes the hours dedicated to interpreting the results of the simulations and its consequences in regards to the topic studied during the development of this thesis. A cost of 28 €/h has been considered because it is the key aspect of the thesis and it is heavily dependant on the work done previously during the *Research* and *Modelling* phases.

5. *Writing.* This includes the hours dedicated to learning LaTeX, writing and revising this thesis. A cost of 9 €/h because this phase is not as technical as others.

Table A.1: Labour costs

Concept	**Hourly rate[€/h]**	**Units** (h)	**Cost**(€)
Research	12	83	996
Modelling	24	140	3360
Simulation	6	27	162
Analysis	28	12	336
Writing	9	64	576
Subtotal		326	5430
VAT(21%)			1140.3
Total			6570.3

B.2 Developement tools and office material

The cost of the equipment and software used during the development of this thesis is included here. The cost of IEEE articles or other literature material is not included, as the university provides free access to those contents.

Amortization for each item is calculated as follows:

1. *Personal computer.* An eight years long life expectancy is considered and five months have been dedicated to the development of this thesis.
2. *Matlab®license.* A year-long license is considered, and five months have been dedicated to the development of this thesis.
3. *PSCAD 4.6.2 EDU.* A year long license is considered, and five months have been dedicated to the development of this thesis.

Table A.2: Development costs

Concept	**Unit cost[€/ut]**	**Units**	**Cost(€)**	**Amortization (€)**
Personal computer	439.90	1	439.90	22.90
MatLab® 2015b (Academic use)	500	1	500	208.30
PSCAD 4.6.2 EDU	400	1	500	166.70
Subtotal				397.90
VAT(21%)				83.60
Total				481.50

B.3 Total cost

Considering the labour costs listed in table A.1 and the development tools and equipment listed in table A.2, the total cost is as seen in table A.3.

Table A.3: Total cost

Item	**Cost[€]**
Labour	6570.30
Development tools and equipment	481.50
Total (VAT included)	**7051.80**

Bibliography

[1] Agustí Egea-Alvarez, Adrià Junyent-Ferré, and Oriol Gomis-Bellmunt. *Active and Reactive Power Control of Grid Connected Distributed Generation Systems*, pages 47–81. Springer Berlin Heidelberg, Berlin, Heidelberg, 2012. i, ii, xi, 21, 22, 23, 24, 25, 26

[2] Red Eléctrica de España. Red de transporte balear. `http://www.ree.es/es/actividades/sistema-electrico-balear/red-de-transporte`. [Online; accessed 27-April-2018]. 1, 13, 17

[3] Red Eléctrica de España. Red de transporte canaria. `http://www.ree.es/es/actividades/sistema-electrico-canario/red-de-transporte`. [Online; accessed 19-June-2018]. 1

[4] Ozan Erdinc, Nikolaos G. Paterakis, and Jo ao P.S. Catalão. Overview of insular power systems under increasing penetration of renewable energy sources: Opportunities and challenges. *Renewable and Sustainable Energy Reviews*, 52:333 – 346, 2015. 1, 2

[5] Red Eléctrica de España. Calidad de servicio. `http://www.ree.es/es/actividades/gestor-de-la-red-y-transportista/calidad-de-servicio`. [Online; accessed 19-June-2018]. 2

[6] E.M.G. Rodrigues, G.J. Osório, R. Godina, A.W. Bizuayehu, J.M. Lujano-Rojas, and J.P.S. Catal ao. Grid code reinforcements for deeper renewable generation in insular energy systems. *Renewable and Sustainable Energy Reviews*, 53:163 – 177, 2016. 2

[7] John Graham and Birger Jonsson. The garabi 2000mw interconnection back-to-back hvdc to connect weak ac systems. 2, 4

[8] M. P. Bahrman. *Overview of HVDC Transmission.* 10 2006. 2, 3

[9] O. E. Oni, I. E. Davidson, and K. N. I. Mbangula. A review of lcc-hvdc and vsc-hvdc technologies and applications. In *2016 IEEE 16th International Conference on Environment and Electrical Engineering (EEEIC)*, pages 1–7, 6 2016. 2, 3

[10] M. P. Bahrman and B. K. Johnson. The abcs of hvdc transmission technologies. *IEEE Power and Energy Magazine*, 5(2):32–44, 3 2007. 3

[11] T. W. May, Y. M. Yeap, and A. Ukil. Comparative evaluation of power loss in hvac and hvdc transmission systems. In *2016 IEEE Region 10 Conference (TENCON)*, pages 637–641, 11 2016. 3

[12] A. Allerhand. A contrarian history of early electric power distribution [scanning our past]. *Proceedings of the IEEE*, 105(4):768–778, 4 2017. 3, 4

[13] W. Long and S. Nilsson. Hvdc transmission: yesterday and today. *IEEE Power and Energy Magazine*, 5(2):22–31, 3 2007. 3

[14] ABB Group. Brazil-Argentina HVDC Interconnection. `http://new.abb.com/systems/hvdc/references/brazil-argentina-hvdc-interconnection`. [Online; accessed 19-April-2018]. 4

[15] G. Morin, L. X. Bui, S. Casoria, and J. Reeve. Modeling of the hydro-quebec-new england hvdc system and digital controls with emtp. *IEEE Transactions on Power Delivery*, 8(2):559–566, 4 1993. 4

[16] H. Bilodeau, S. Babaei, B. Bisewski, J. Burroughs, C. Drover, J. Fenn, B. Fardanesh, B. Tozer, B. Shperling, and P. Zanchette. Making old new again: Hvdc and facts in the northeastern united states and canada. *IEEE Power and Energy Magazine*, 14(2):42–56, 3 2016. 4

[17] Red Eléctrica de España. Rómulo: Interconnexió Elèctrica Península-Balears. `http://www.ree.es/es/actividades/proyectos-singulares/interconexion-peninsula-baleares`. [Online; accessed 23-April-2018]. 4

[18] R. D. Zimmerman, C. E. Murillo-Sanchez, and R. J. Thomas. Matpower: Steady-state operations, planning, and analysis tools for power systems research and education. *IEEE Transactions on Power Systems*, 26(1):12–19, Feb 2011. 5, 8, 17, 30

[19] R. D. Zimmerman, C. E. Murillo-Sanchez, and R. J. Thomas. *MATPOWER 6.0 User's Manual*. Power Systems Engineering Research Center, Feb 2016. 9

[20] Industria y Competitividad Ministerio de Economía. Real decreto 1039/2017, de 15 de diciembre, por el que se declaran oficiales las cifras de población resultantes de la revisión del padrón municipal referidas al 1 de enero de 2017. *Boletín Oficial del Estado*, (316):130530–130535, 12 2017. 13

[21] Instituto Nacional de Estadística. Balears, Illes: Población por Municipios y Sexo. `http://www.ine.es/jaxiT3/Tabla.htm?t=2860&L=0`. [Online; accessed 26-April-2018]. 13, 16

[22] Red Eléctrica de España. Demanda Balear en Tiempo Real. `http://www.ree.es/es/actividades/sistema-electrico-balear/demanda-de-energia-en-tiempo-real`. [Online; last accessed 04-June-2018. Used information for February 5th, 2018.]. 16

[23] P. Kundur. *Power System Stability and Control*. New York : McGraw-Hill, 1994. 21, 22, 32, 35, 36

[24] Se-Kyo Chung. A phase tracking system for three phase utility interface inverters. *IEEE Transactions on Power Electronics*, 15(3):431–438, May 2000. 25

[25] J. C. Vasquez, J. M. Guerrero, A. Luna, P. Rodriguez, and R. Teodorescu. Adaptive droop control applied to voltage-source inverters operating in grid-connected and islanded modes. *IEEE Transactions on Industrial Electronics*, 56(10):4088–4096, 10 2009. 29

[26] C. T. Lee, C. C. Chu, and P. T. Cheng. A new droop control method for the autonomous operation of distributed energy resource interface converters. *IEEE Transactions on Power Electronics*, 28(4):1980–1993, 4 2013. 29

[27] W. Yao, M. Chen, J. Matas, J. M. Guerrero, and Z. M. Qian. Design and analysis of the droop control method for parallel inverters considering the impact of the complex impedance on the power sharing. *IEEE Transactions on Industrial Electronics*, 58(2):576–588, 2 2011. 29

[28] Paul C Krause. *Analysis of Electric Machinery and Drive Systems*. New York : McGraw-Hill, 1986. Includes bibliographical references and index. 32, 33